Polymerization of Olefins Through Heterogeneous Catalysis. VI. Effect of Particle Heat and Mass Transfer on Polymerization Behavior and Polymer Properties

S. FLOYD, TOMI HEISKANEN, T. W. TAYLOR, G. E. MANN, and W. H. RAY, *Department of Chemical Engineering, University of Wisconsin, Madison, Wisconsin 53706*

Synopsis

The multigrain model for polymerization of olefins over solid catalysts is used to predict kinetic behavior, molecular weights, and polydispersities. The effects of intraparticle and external boundary layer transport resistance on the kinetic behavior and polymer properties are explored. Means for the experimental detection of intraparticle diffusion resistance are suggested. The importance of catalyst physical properties, such as the porosity, and the catalyst loading is illustrated through simulation. Finally, the hypotheses of diffusion resistance and site heterogeneity as explanations for the broad molecular weight distributions of olefin polymers are critically evaluated, and molecular weight distribution control in industrial catalysts is discussed.

INTRODUCTION

In studies of polymerization of olefins over solid catalysts, the potential for intraparticle diffusion resistance to influence the rate of polymerization and polymer properties has been recognized for some time. In previous papers by this group (e.g., Refs. 1–6), the multigrain model for polymerization over solid catalysts was developed. Early on, the model was used to illustrate the possibility for diffusion-controlled reaction, and broadening of the molecular weight distribution due to steep concentration gradients in the growing polymer particle.[1] Subsequently, some experimental evidence was presented which was suggestive of intraparticle diffusion limitations.[7] More recently, the parameters of the multigrain model were subjected to detailed analysis, and ranges for these parameters (most importantly, the diffusivities in the porous polymer particle and in the semicrystalline polymer itself) were determined.[4,5] In addition, quantitative criteria for the existence of heat and mass transfer resistances in solid-catalyzed systems have been presented in graphical form, so that their significance can be determined for catalysts of arbitrary activity.[4,5] It is the purpose of the present paper to demonstrate through simulations using the multigrain model the influence of heat and mass transfer on the polymerization behavior of solid catalysts. Experimental means for detection of diffusion resistance in polymerization will be discussed, as well as the importance of catalyst physical properties. Also, the much-debated issue of diffusion-induced broadening of the molecular weight distri-

Journal of Applied Polymer Science, Vol. 33, 1021–1065 (1987)
 CCC 0021-8995/87/041021-45$04.00

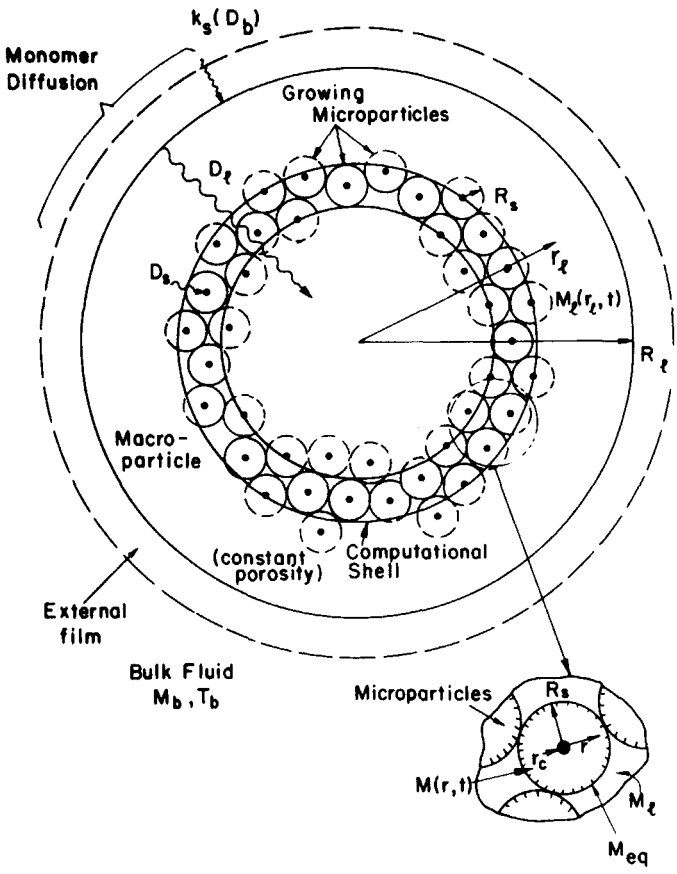

Fig. 1. The multigrain model.

bution (MWD) will be treated, using the best estimates available for the key model parameters. The potential of site heterogeneity to broaden the MWD will then be analyzed in detail, and its practical aspects will be discussed.

MODEL DEVELOPMENT

In this section, the multigrain model incorporating site heterogeneity and molecular weight calculations will be described. The model is schematically illustrated in Figure 1. The model structure is based on numerous observations (e.g., Refs. 8–10) that the original catalyst particle breaks up into smaller subunits, around which polymer growth takes place. Thus, the large polymer macroparticle is comprised of many small microparticles, which encapsulate the catalyst fragments. All of the microparticles at a given macroparticle radius are assumed to be the same size. For monomer to reach the active sites, it must diffuse through the macropores between the microparticles, and then through the semicrystalline polymer of the microparticles themselves. Realistic values for the diffusivities in these regimes and other parameters of interest are presented in Table I.

TABLE I
Range of Multigrain Model Parameters for Polymerization of Propylene and Ethylene under Industrial Conditions[4]

Property	Propylene (PP)		Ethylene (PE)	
	Slurry (*n*-heptane)	Gas	Slurry (*n*-hexane)	Gas
M_b (mol/L)	4.0	1.0	2.0	1.0
T_b (K)	343	343	353	353
P (atm)	11	21	28	27
mol fraction monomer	0.49	1	0.266	1
$-\Delta H_p$ (kcal/mol)	20.5	24.8	22.7	25.7
E (kcal/mol)	10	10	10	10
k_p (L/mol-site · s) (High activity catalyst)	660–2640	2640	2000–4000	4000
C_* (mol-sites/L-cat)	10^{-3}–10^{-1}	10^{-3}–10^{-1}	10^{-3}–10^{-1}	10^{-3}–10^{-1}
k_e (cal/cm · s · k)	3.5×10^{-4}	2.6×10^{-4}	5.6×10^{-4}	4.8×10^{-4}
D_b (cm^2/s)	8×10^{-5}	4×10^{-3}	1×10^{-4}	6.0×10^{-3}
D_ℓ (cm^2/s)	10^{-6}–10^{-5}	10^{-4}–10^{-3}	10^{-6}–10^{-5}	10^{-4}–10^{-3}
D_s (cm^2/s)	10^{-8}–10^{-6}	10^{-8}–10^{-6}	10^{-8}–10^{-6}	10^{-8}–10^{-6}
R_s (cm)	10^{-6}–10^{-4}	10^{-6}–10^{-4}	10^{-6}–10^{-4}	10^{-6}–10^{-4}
R_ℓ (cm)	10^{-4}–0.1	10^{-4}–0.1	10^{-4}–0.1	10^{-4}–0.1

Notation:

M_b:	Bulk monomer concentration
T_b:	Bulk temperature
$-\Delta H_p$:	Heat of polymerization
k_p:	Propagation rate constant
C_*:	Active site concentration
k_e:	Effective thermal conductivity of polymer particle
D_b:	Bulk diffusivity of monomer
D_ℓ:	Large particle diffusivity
D_s:	Small particle diffusivity
R_s:	Small particle radius
R_ℓ:	Large particle radius

To model the particle, we must write the partial differential equations for the monomer concentration and temperature in the two regions. From the concentration and temperature profiles we may calculate the reaction rates, yields, and molecular weight distribution.

The governing equation for the diffusion of monomer in the macroparticle is

$$\epsilon_\ell \frac{\partial M_\ell}{\partial t} = \frac{1}{r_\ell^2} \frac{\partial}{\partial r_\ell} \left(D_\ell r_\ell^2 \frac{\partial M_\ell}{\partial r_\ell} \right) - R_v \tag{1}$$

where ϵ_ℓ is the large particle porosity, $M_\ell(r_\ell, t)$ is the monomer concentration in the pores of the macroparticle, and D_ℓ is the pseudobinary macrodiffusion coefficient. The reaction rate term, R_v, represents the total rate of consumption of monomer in an infinitesimal spherical shell at a given radius of the

macroparticle. The boundary and initial conditions are

$$r_\ell = 0 \qquad \frac{\partial M_\ell}{\partial r_\ell} = 0 \tag{2}$$

$$r_\ell = R_\ell \qquad D_\ell \frac{\partial M_\ell}{\partial r_\ell} = k_s(M_b - M_\ell) \tag{3A}$$

or

$$r_\ell = R_\ell \qquad M_\ell = M_S \tag{3B}$$

$$t = 0 \qquad M_\ell = M_{\ell 0} \tag{4}$$

where M_b is the bulk monomer concentration in the reactor, k_s is the mass transfer coefficient in the external film, and M_S is the monomer concentration at the external solid surface. For the microparticles, the particle differential equation governing monomer diffusion is given as

$$\epsilon_s \frac{\partial M}{\partial t} = \frac{1}{r^2} \frac{\partial}{\partial r}\left(D_s r^2 \frac{\partial M}{\partial r} \right) \qquad r_c \le r \le R_s \tag{5}$$

where $M(r, t)$ is the monomer concentration in the microparticle, D_s is the pseudobinary microdiffusion coefficient, and ϵ_s is the porosity. In the microparticles, all of the active sites are assumed to be at the surface of the catalyst core at $r = r_c$. Thus, the boundary and initial conditions are given by

$$r = r_c \qquad 4\pi r_c^2 D_s \frac{\partial M}{\partial r} = \frac{4}{3}\pi r_c^3 R_{cs} \tag{6}$$

$$r = R_s \qquad M = M_{\text{eq}},\ M_{\text{eq}}(M_\ell) \le M_\ell \tag{7}$$

$$t = 0 \qquad M = M_{s0} \tag{8}$$

where boundary condition (7) allows for the possibility of sorption equilibrium at the surface of the microparticles. Here r_c is the catalyst primary particle radius, R_s is the microparticle radius, and R_{cs} is the rate of polymerization at the catalyst particle surface given by

$$R_{cs} = \sum_{i=1}^{N} k_{pi} C_{*i} M_c = k_p C_* M_c \tag{9}$$

where $k_p C_* = \sum_{i=1}^{N} k_{pi} C_{*i}$ is an effective rate parameter and M_c is the monomer concentration at the catalyst surface. Here, the summation accounts for N types of active sites. The propagation rate constant and active site concentrations of site i are k_{pi} and C_{*i}, respectively. The partial differential equations for the energy balances in the macroparticles and the microparticles are completely analogous to (1)–(8) and are shown in Ref. 4. From consideration of the time constants for equilibration of heat and mass transfer in the

system, it was determined[4] that the quasi-steady-state approximation could be applied to the microparticle diffusion Eq. (5). By substituting the boundary conditions, one obtains the resulting analytic solution for the monomer concentration at the catalyst surface as

$$M_c = \frac{M_{eq}(M_\ell)}{1 + \frac{k_p C_*}{3D_s} r_c^2 \frac{R_s - r_c}{R_s}} \tag{10}$$

The multigrain model solves for the concentration profile in the macroparticle and the monomer concentration at the catalyst surface using Eq. (10) for each radial shell shown in Figure 1. Although earlier versions of the multigrain model have been described previously,[1,2] we shall review the new features of the current version of the Multigrain Model Program. As an option, one may assume the large particle diffusivity D_ℓ to be large, and skip the numerical solution for the large particle. This assumption is believed to be generally valid for gas phase polymerization.[4] Also, the molecular weight calculations described below may be omitted for a considerable computation time saving, if these are not needed. In the program, one may have one or multiple active sites ($N > 1$ in Eq. (9)), which may decay independently with first or second-order kinetics. The sum of the contributions of these sites appears in the overall rate, yield and molecular weights. The M_w and $Q = M_w/M_n$ values for polymer produced at each site type are also calculated.

In solid-catalyzed polymerizations, the polymer grows at the active sites of the catalyst until chain transfer occurs, or until the site is deactivated. Thus, there is present "live" polymer, which is still attached to an active site, and "dead" polymer, which has at its end a group from a chain transfer or deactivating agent. The moments of the live and dead polymer can be calculated, using the method outlined by Ray.[11,12] The application of the method for solid-catalyzed olefin polymerization is described below.

The prediction of polymer molecular weight distributions assuming multiple active sites on the surface of the catalyst has been reported by several authors.[13-16,32] Bohm,[32] Keii et al.,[13] and Heiskanen[14] have used a model without diffusion limitations, while Galvan and Tirrell[15] have used an expansion or flow model which allows only one level of diffusion. Our work (Ref. 16 and the present paper) makes use of the multigrain model which allows polymer particle microstructure and two levels of diffusion. The modeling equation for this formulation are described in what follows.

For the live polymer at the k-th active site ($k = 1, \ldots, N$), the ℓth moment is

$$\lambda_\ell^k = \sum_{i=1}^{\infty} i^\ell P_i^k \tag{11}$$

where P_i^k is the concentration of live polymer of chain length i. For the dead polymer, the ℓ-th moment is defined as

$$\Lambda_\ell^k = \sum_{i=1}^{\infty} i^\ell M_i^k \tag{12}$$

where M_i^k is the concentration of dead polymer of chain length i. From these definitions, the number average molecular weight produced by the k-th site, M_n^k, is the sum of live and dead polymer and is given by

$$M_n^k = \frac{\lambda_1^k + \Lambda_1^k}{\lambda_0^k + \Lambda_0^k}\text{MW} \tag{13}$$

where MW is the molecular weight of the monomer. Similarly, the weight average molecular weight of polymer produced by the k-th site, M_w^k, is given by

$$M_w^k = \frac{\lambda_2^k + \Lambda_2^k}{\lambda_1^k + \Lambda_1^k}\text{MW} \tag{14}$$

hence the polydispersity at site k becomes

$$Q^k = \frac{\left(\lambda_2^k + \Lambda_2^k\right)\left(\lambda_0^k + \Lambda_0^k\right)}{\left(\lambda_1^k + \Lambda_1^k\right)^2} \tag{15}$$

Knowing the weight fractions of polymer produced over active site k, $w_k = \lambda_1^k / \sum_{j=1}^{N} \lambda_1^j$, the cumulative molecular weight and polydispersity of the total polymer produced may be found from

$$M_n = \frac{1}{\sum_{k=1}^{N} w_k / M_n^k} \tag{16}$$

$$M_w = \sum_{k=1}^{N} w_k M_w^k \tag{17}$$

$$Q = M_w / M_n = \sum_{k=1}^{N} w_k M_w^k \cdot \sum_{k=1}^{N} w_k / M_n^k \tag{18}$$

The problem of determining the polymer properties has thus been changed to one of calculating the zeroth, first, and second moments. On taking the derivative of the zeroth moment of live polymer at site k, we obtain

$$\frac{d\lambda_0^k}{dt} = \frac{d}{dt}\sum_{i=1}^{\infty} P_i^k = \sum_{i=1}^{\infty} \frac{dP_i^k}{dt} \tag{19}$$

where from propagation and chain transfer kinetics we get

$$\frac{dP_i^k}{dt} = k_p^k M_c P_{i-1}^k - k_p^k M_c P_i^k - k_{tr}^k Tr P_i^k \tag{20}$$

Here the overall chain transfer rate is defined as the sum of monomer, alkyl,

and hydrogen chain transfer rates,

$$k_{Tr}^k Tr = k_M^k M_c + k_A^k A^{1/2} + k_H^k H^{1/2} \tag{21}$$

We may define the probability of propagation for site k as

$$\alpha_k = \frac{k_p^k M_c P_i^k}{k_{Tr}^k Tr P_i^k + k_1^k M_c P_i^k} = \frac{k_p^k M_c}{k_{Tr}^k Tr + k_p^k M_c} \tag{22}$$

Rewriting (20) as

$$\frac{dP_i^k}{dt} = k_p^k M_c \left(P_{i-1}^k - P_i^k / \alpha_k \right) \tag{23}$$

and summing for all i gives

$$\frac{d\lambda_0^k}{dt} = k_p^k M_c \left(\sum_{i=1}^{\infty} P_{i-1}^k - \sum_{i=1}^{\infty} P_i^k / \alpha_k \right) \tag{24}$$

but since by definition

$$\lambda_0^k = \sum_{i=1}^{\infty} P_i^k \qquad C_*^k = \sum_{i=0}^{\infty} P_i^k \tag{25}$$

we obtain

$$\frac{d\lambda_0^k}{dt} = k_p^k M_c \left(C_*^k - \lambda_0^k / \alpha_k \right) \tag{26}$$

Note that from Eq. (25), we assume that P_0^k is the concentration of vacant sites of type k.

Turning to the dead polymer, we see that polymer of chain length i is formed solely by the chain transfer reactions with live polymer of chain length i. Hence,

$$\frac{dM_i^k}{dt} = k_{Tr}^k Tr P_i^k \qquad i = 2, 3, \ldots, \infty \tag{27}$$

and from the definition

$$\Lambda_0^k \equiv \sum_{i=2}^{\infty} M_i^k \tag{28}$$

we obtain

$$\frac{d\Lambda_0^k}{dt} = k_p^k M_c (1/\alpha_k - 1) \sum_{i=2}^{\infty} P_i^k = k_p^k M_c \left(\frac{1}{\alpha_k} - 1 \right) \left[\lambda_0^k - P_1^k \right] \tag{29}$$

where P_1^k is a monomer molecule bonded to an active site, k. Obviously, in

order to solve for Λ_0^k, an expression for $P_1^k(t)$ is needed. This is obtained as

$$\frac{dP_1^k}{dt} = k_p^k M_c P_0^k - k_p^k M_c P_1^k - k_{Tr}^k Tr P_1^k + k_M^k M_c \lambda_0^k \tag{30}$$

Recalling that

$$P_0^k = C_*^k - \lambda_0^k \tag{31}$$

Eq. (30) may be rewritten as

$$\frac{dP_1^k}{dt} = k_P^k M_c\left(C_*^k - \lambda_0^k - P_1^k/\alpha_k\right) \tag{32}$$

The procedures used to calculate the zeroth moments are also applicable to higher moments. The derivations, which require a few more algebraic manipulations, will not be shown here. For the live polymer moments, the resulting expressions for the first and second moments are

$$\frac{d\lambda_1^k}{dt} = k_p^k M_c\left[C_*^k + (1 - 1/\alpha_k)\lambda_1^k\right] \tag{33}$$

$$\frac{d\lambda_2^k}{dt} = k_p^k M_c\left[(1 - 1/\alpha_k)\lambda_2^k + 2\lambda_1^k + C_*^k\right] \tag{34}$$

while for the dead polymer moments

$$\frac{d\Lambda_1^k}{dt} = k_p^k M_c(1/\alpha_k - 1)\left(\lambda_1^k - P_1^k\right) \tag{35}$$

$$\frac{d\Lambda_2^k}{dt} = k_p^k M_c(1/\alpha_k - 1)\left(\lambda_2^k - P_1^k\right) \tag{36}$$

From comparison of the time constants of the moment equations and Eq. (32) for P_1, it was determined that the quasi-steady-state assumption could be applied to the zeroth live moment and P_1. This is equivalent to assuming that the chain lifetime is short relative to the time scale for accumulation of polymer product (i.e., reactor residence time).

To calculate the polymer properties, M_n^k and polydispersity at each site are calculated at each time step. The moment equations are integrated over time for each shell, and the contributions of each shell are summed. The moment equations in each shell may be written in matrix form as

$$\frac{d\mathbf{y}^k}{dt} = \mathbf{C}\mathbf{y}^k + \mathbf{d} \tag{37}$$

where $\mathbf{C}$ and $\mathbf{d}$ are the appropriate coefficients and

$$\left(\mathbf{y}^k\right)^T = \left[\lambda_0^k, \lambda_1^k, \lambda_2^k, \Lambda_0^k, \Lambda_1^k, \Lambda_2^k, P_1^k\right] \tag{38}$$

In order to solve Eq. (37), (i.e., either seven (without the QSSA) or five (with QSSA for λ_0^k, M_1^k) ODEs), a backwards Euler method[17] was employed. Thus, the implicit approximation

$$\frac{\Delta \mathbf{y}^k}{\Delta t} = \mathbf{C}(\mathbf{y}_n^k + \Delta \mathbf{y}^k) + \mathbf{d} \tag{39}$$

is made, where $\mathbf{y}_n^k = \{\mathbf{y}^k \text{ at time } t = n\Delta t\}$. Then, (39) can be transformed to the linear system

$$(\mathbf{I} - \mathbf{C}\Delta t)\Delta \mathbf{y}^k = (\mathbf{C}\mathbf{y}_n^k + \mathbf{d})\Delta t \tag{40}$$

which is solved using LINPACK,[18] yielding the new moment values at time $t + \Delta t$ as

$$\mathbf{y}_{n+1}^k = \mathbf{y}_n^k + \Delta \mathbf{y}^k \tag{41}$$

There were no instability problems using this method. For more details of the computational procedure see Ref. 16.

MASS TRANSFER EFFECTS ON POLYMERIZATION KINETICS

In Ref. 4, graphical criteria were developed for determining significant heat and mass transfer at the microparticle and macroparticle level. According to these criteria, intraparticle temperature gradients are only likely to be significant for large particles of very high activity catalyst in gas phase polymerization, and these conditions are not considered in the present work. In slurry polymerization, on the other hand, mass transfer effects in the macroparticle are frequently significant, especially early in the polymerization. This comes about because in the initial stages of polymerization, the volumetric rate of reaction is at a maximum and the surface area exposed to the monomer source (the bulk liquid phase) is at a minimum. The effects of intraparticle mass transfer will be most pronounced for large particles of catalyst, and high catalyst activities. Besides the intraparticle mass transfer resistance in the pores of the growing polymer particle, there also exists a mass transfer resistance in the semicrystalline polymer of the microparticles. While the former will decrease with time as the volumetric reaction rate decreases, the latter will increase slightly with time as the polymer film surrounding the active sites becomes thicker. The multigrain model solves for both the concentration profile in the macroparticle, and the concentration drop across the polymer film in the microparticles. Although mass transfer at the microparticle level should become limiting for some combinations of catalyst activity and physical conditions, especially for poor break-up of catalyst, mass transfer resistance in the pores of the macroparticle appears to be of more general significance,[4,6] and will be the primary concern in this paper. As mentioned above, the macroparticle mass transfer resistance is at a maximum at the beginning of polymerization. Thus, in the absence of catalyst deactivation and microparticle diffusion resistance, an acceleration-type rate behavior

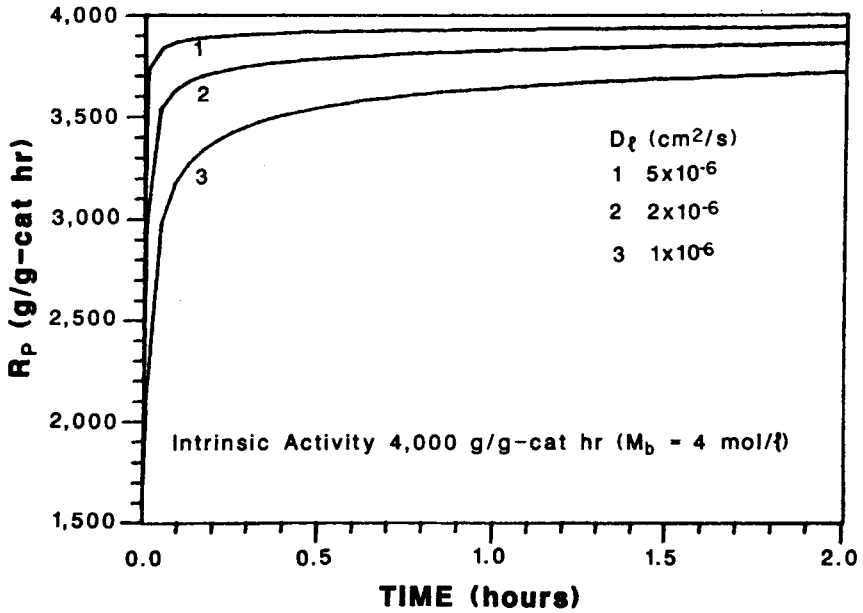

Fig. 2. Rate curves for nondeactivating catalysts with varying degrees of macroparticle diffusion resistance. Propylene polymerization, $k_p = 660$ L/mol · s, $C_* = 10^{-5}$ mol/g-cat, $M_b = 4$ mol/L.

would be predicted, not a decay type. This is illustrated in Figure 2 for a catalyst of constant intrinsic activity 4000 g/g-cat · h at $M_b = 4$ mol/L, with varying degrees of macroparticle diffusion resistance, which is determined by the large particle diffusivity D_ℓ. Here and throughout this paper, external film mass and heat transfer effects have been included, using the Ranz-Marshall correlation[5] for the heat and mass transfer coefficients. As seen from Figure 2, the acceleration behavior becomes more pronounced as the diffusivity decreases and diffusion resistance becomes more severe. At a diffusivity of $D_\ell = 5 \times 10^{-6}$ cm²/s, the observed activity is close to the intrinsic activity, but at $D_\ell = 1 \times 10^{-6}$ cm²/s, there is significant diffusion resistance throughout the two hour period. Figure 3 illustrates that when $D_\ell = 5 \times 10^{-6}$ cm²/s, near kinetic control is observed for a deactivating catalyst with average activity 4000 g/g-cat · h. At this diffusivity value, a nondeactivating catalyst producing the same yield exhibits a virtually constant rate.

In the past, it was believed that the rate decay might result from increasing diffusion resistance as the polymer grows around the active sites. However, experimental evidence has been presented for both gas and slurry systems, which denies diffusion resistance as the source of the rate decay. In experiments in which the monomer supply was temporarily interrupted, the polymerization rate either continued to decay during the interruption[19-22] or resumed at a higher rate,[23] whereas it would be expected to resume at the same rate observed prior to interruption if diffusion resistance were responsible for the decay. Although it is possible that microparticle diffusion resistance can lead to decay-type behavior for relatively large catalyst grain sizes and very high catalyst activities (e.g., Ref. 1), it has been found[4] that the

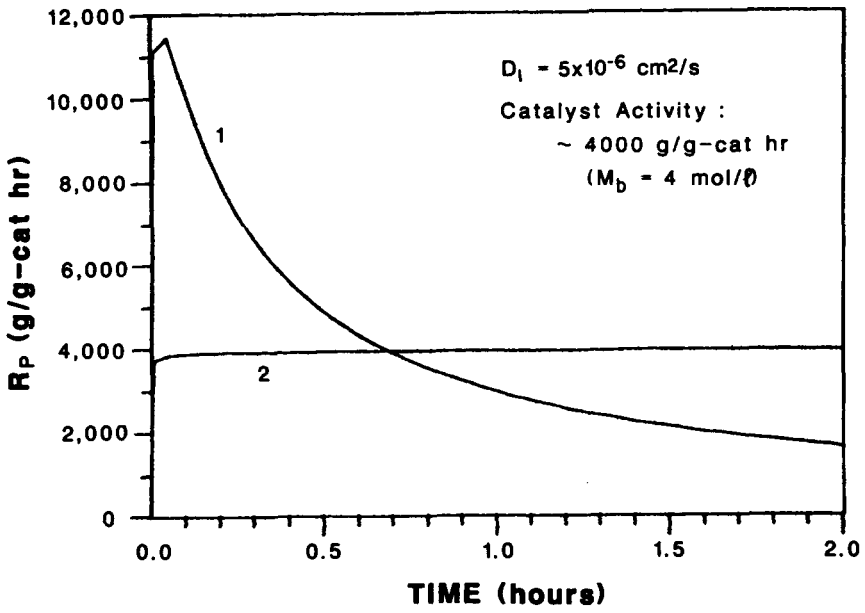

Fig. 3. Rate curves for high activity catalysts under near kinetic control. (1) Second-order deactivating catalyst, k_p = 2460 L/mol · s, $C_*(0) = 10^{-5}$ mol/g-cat, $t_{1/2}$ = 0.25 hours, yield = 7880 g/g-cat; (2) Nondeactivating catalyst, k_p = 660 L/mol · s, $C_*(0) = 10^{-5}$ mol/g-cat, yield = 7850 g/g-cat.

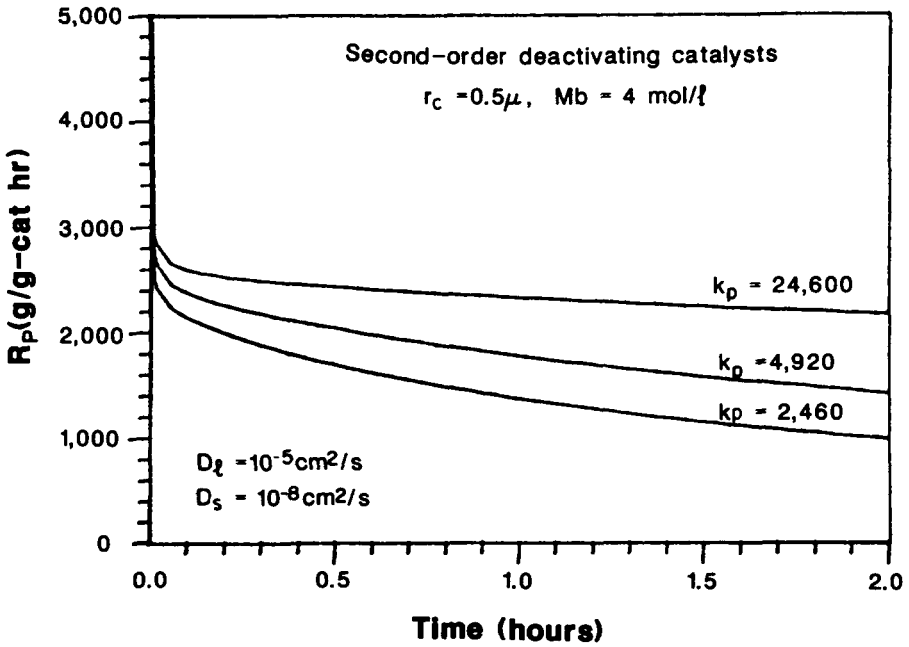

Fig. 4. Rate curves for second-order deactivating catalysts with varying degrees of microparticle diffusion resistance. (1) k_p = 2460 L/mol · s, Y_2 = 2911 g/g-cat; (2) k_p = 4920 L/mol · s, Y_2 = 3665 g/g-cat; (3) k_p = 24600 L/mol · s, Y_2 = 4712 g/g-cat. All catalysts: $C_*(0) = 10^{-5}$ mol/g-cat, $t_{1/2}$ = 0.25 hours.

monomer concentration at the catalyst surface is relatively insensitive to the microparticle growth factor ϕ_g when $\phi_g > \sim 5$. Because the time scale for growth of the microparticle to $\phi_g > 5$ is very short for modern catalysts, the polymerization rate would be observed to be almost constant from the beginning of polymerization under conditions where microparticle diffusion is limiting. For deactivating catalysts, the decay is compensated for by diffusion so that the rate will appear to decay slower than the actual decay kinetics in the presence of microparticle diffusion resistance. This is illustrated in Figure 4 for second-order deactivating catalysts with a half-life of 0.25 hours when the catalyst grain size, $r_c = 0.5$ μm. This value of r_c is rather large for propylene catalysts, however, some ethylene catalysts have this value or larger. Unless otherwise stated, for all other simulations in this paper, the value of r_c was 0.01 μm. For catalyst 1 in Figure 4 (observed productivity ~ 4000 g/g-cat · h over 2 hours, the effectiveness factor is 71%, while for catalysts 2 and 3 (2 and 10 times as active) the effectiveness factors are 44% and 11.5%, respectively. Catalyst 1 has the same kinetic parameters as the second-order deactivating catalyst in Figure 3, and it is seen that the rate decay is not as pronounced in the presence of microparticle diffusion resistance. With catalyst 3, an almost constant rate is observed.

When there is significant diffusion resistance in the macroparticle, the effect of catalyst decay on the rate is again offset by increasing penetration of monomer into the growing particle. Thus, the observed order of rate decay will be less than the true order in this circumstance. Under severe diffusion influence, hybrid-type rate curves may result, as illustrated in Figures 5 and 6.

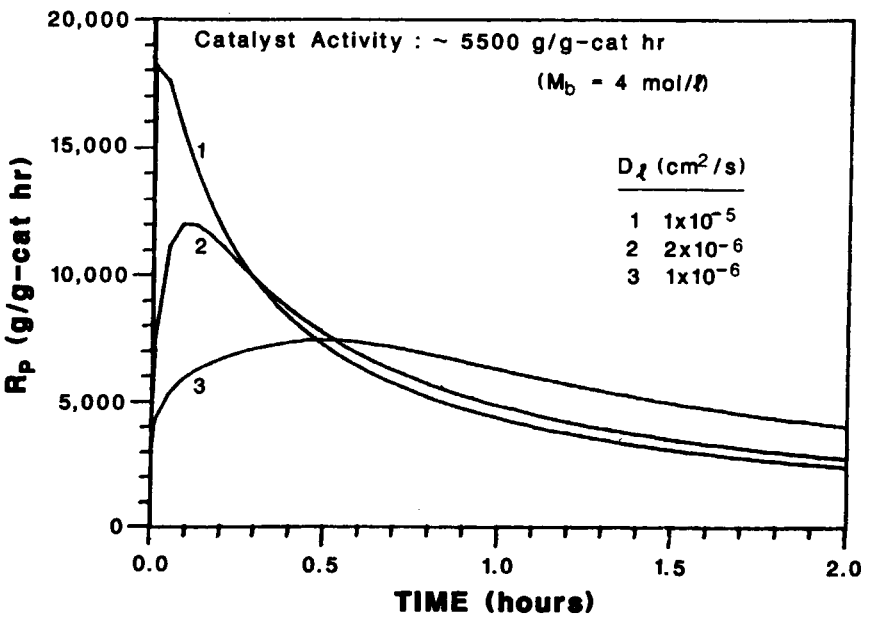

Fig. 5. Rate curves for first-order deactivating catalysts with varying degrees of macroparticle diffusion resistance. (1) $k_p = 2640$ L/mol · s, $Y_2 = 10{,}600$ g/g-cat; (2) $k_p = 3100$ L/mol · s, $Y_2 = 10{,}800$ g/g-cat; (3) $k_p = 4800$ L/mol · s, $Y_2 = 10{,}900$ g/g-cat. All catalysts: $C_*(0) = 10^{-5}$ mol/g-cat, $t_{1/2} = 0.5$ hours.

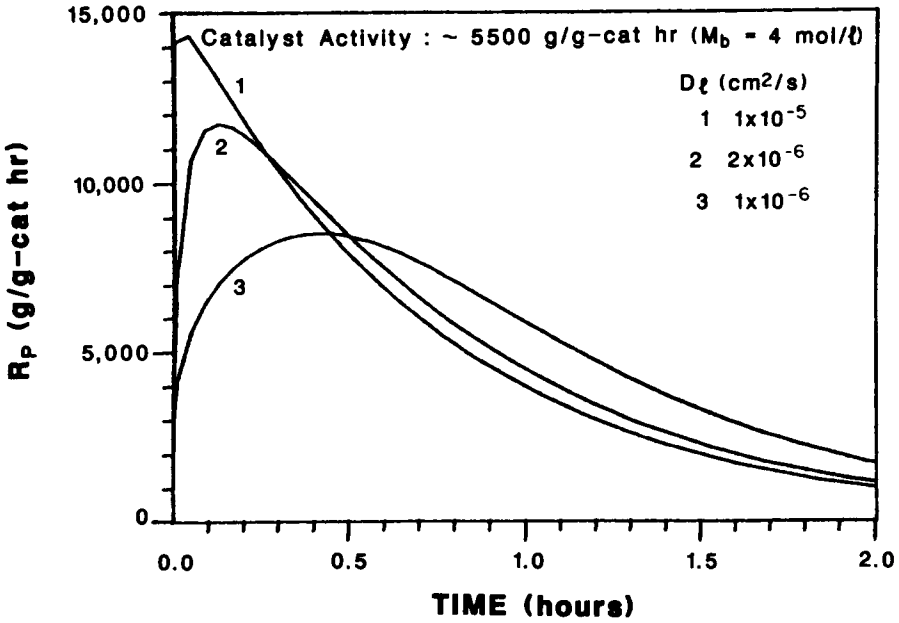

Fig. 6. Rate curves for second-order deactivating catalysts with varying degrees of macroparticle diffusion resistance. (1) k_p = 3600 L/mol · s, Y_2 = 11,700 g/g-cat; (2) k_p = 4200 L/mol · s, Y_2 = 11,600 g/g-cat; (3) k_p = 6600 L/mol · s, Y_2 = 11,800 g/g-cat. All catalysts: $C_*(0) = 10^{-5}$ mol/g-cat, $t_{1/2}$ = 0.25 hours.

These figures are for first- and second-order deactivating catalysts, respectively, with comparable average activity over a two-hour period but experiencing different degrees of diffusion influence due to different values of the large particle diffusivity. Acceleration and hybrid-type rate behavior have frequently been observed, especially for the polymerization of ethylene,[24-28] but also with classical catalyst systems,[29] at low monomer concentration. It is especially noteworthy that decay-type behavior has been observed for propylene polymerization while acceleration-type behavior was observed for ethylene polymerization over the same catalyst.[25] The ratio of yields of polyethylene to polypropylene was roughly 50 : 1. In general, the ratio of the rate of reaction of ethylene to propylene over the same catalyst ranges from around 30 to as high as 500.[30,31] Of course, non-decay-type rate behavior may also be explained through a chemical mechanism, with a slow initiation step for active sites.

General criteria for intraparticle diffusion resistance have been presented in Ref. 4. One major conclusion from that analysis was that mass transfer resistance is most severe early in the polymerization and decreases as the polymer particle grows in size. This produces an interesting effect which is somewhat subtle. For a given intrinsic catalyst activity, the diffusion resistance will be greater at any given polymerization time for lower bulk monomer concentrations. This is simply because lower bulk monomer concentrations cause the polymer particles to grow more slowly and thus the period of mass transfer resistance endures longer.

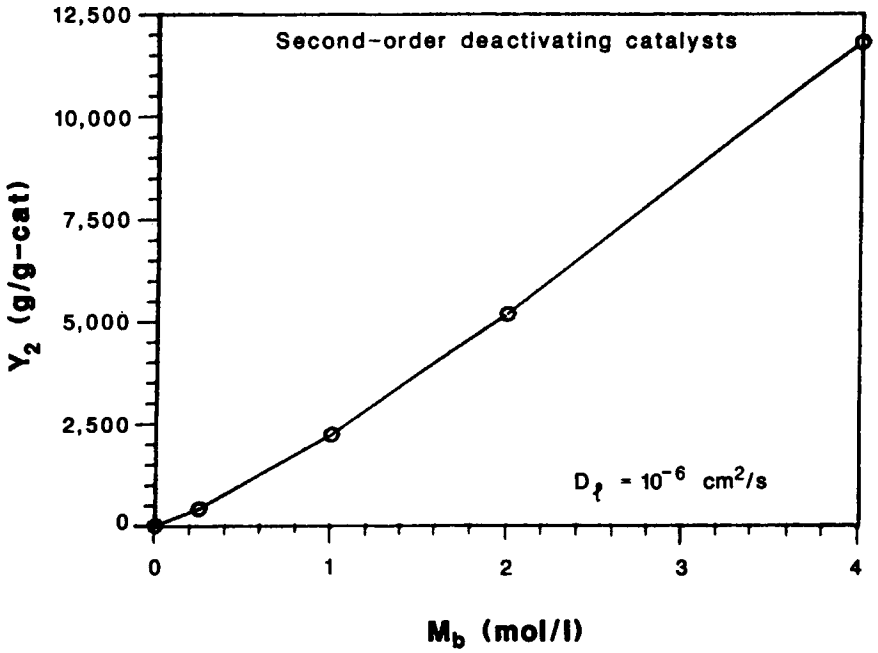

Fig. 7. Plot of yield vs. monomer concentration for second-order deactivating catalyst under diffusion control. k_p = 6600 L/mol · s, $C_*(0) = 10^{-5}$ mol/g-cat, $t_{1/2}$ = 0.25 hours.

Thus for nondeactivating catalysts, in a fixed time period, the diffusion resistance experienced will be more severe if the bulk concentration is low. This has the consequences that (1) In the presence of severe diffusion resistance, the reaction rate will be nonlinear in the concentration; (2) Catalysts tested for a fixed time period at or near atmospheric pressure, will show more diffusion resistance than under actual process conditions.

Figure 7 illustrates a nonlinear concentration effect at low bulk monomer concentration for a high activity, second-order decaying catalyst. Bohm[32] has shown plots resembling this for ethylene polymerization over Hoechst catalyst, and examples also appear in Ref. 29 (pp. 33, 154) for polymerizations at subatmospheric pressures.

EFFECTS OF CATALYST PHYSICAL PROPERTIES

With high activity catalysts in current use, the physical properties as well as the chemical properties need to be considered. In particular, the catalyst particle size, the microparticle size, and the porosity are of importance. With respect to the first factor, the use of large particle sizes with catalysts of high activity can lead to diffusion-controlled reaction. Figure 8 shows the ratio of yields expected from catalyst particles of 20 and 100 μm diameter as a function of the macroparticle diffusivity, at a bulk monomer concentration of 4 mol/L. Figure 9 illustrates the predictions when the monomer concentration is reduced of M_b = 0.5 mol/L. This monomer concentration roughly corresponds to atmospheric pressure of propylene in heptane at 50°C. In each case, the ratio of yields at 0.5 and 3 hours is illustrated for a catalyst of activity

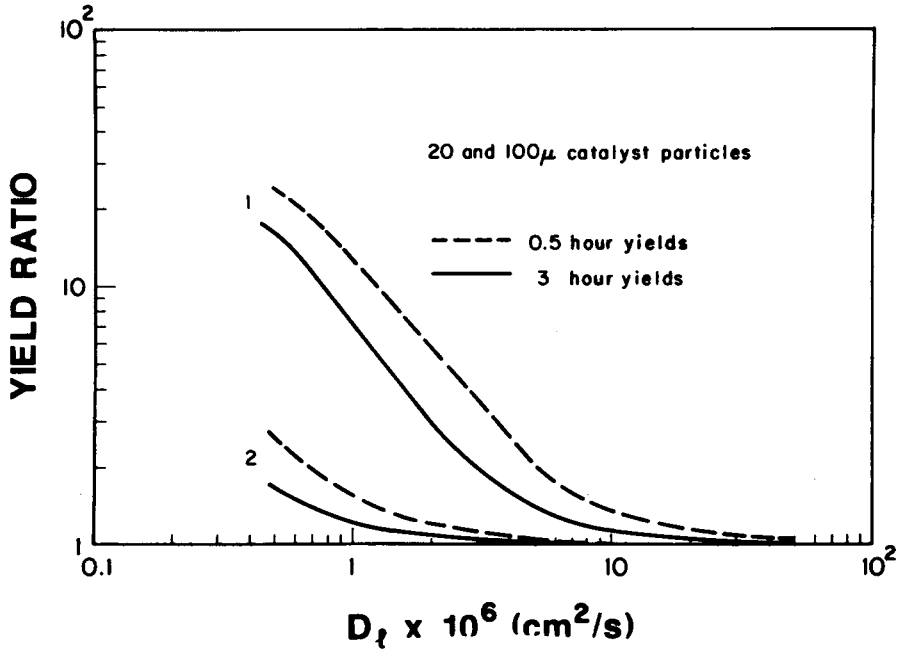

Fig. 8. Ratio of yields of 20 μm and 100 μm catalyst particles of first-order deactivating catalysts as a function of macroparticle diffusivity D_1, at high monomer concentration (M_b = 4 mol/L). (1) k_p = 1000 L/mol · s, r_c = 0.01 μm; (2) k_p = 60 L/mol · s, r_c = 0.1 μm, $C_*(0) = 10^{-5}$ mol/g-cat, $t_{1/2}$ = 3 hours.

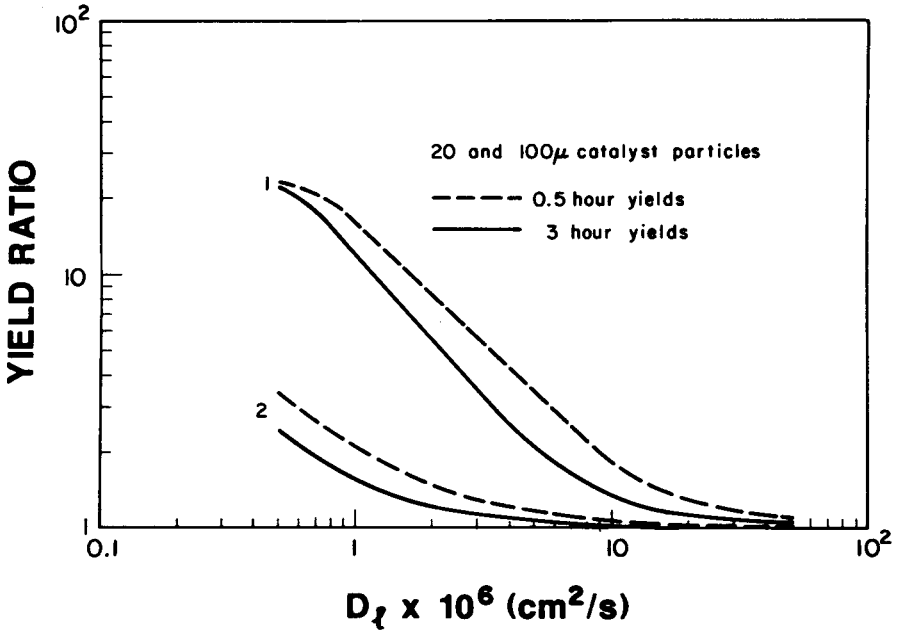

Fig. 9. Ratio of yields of 20 μm and 100 μm catalyst particles of first-order deactivating catalysts as a function of macroparticle diffusivity D_1, at low monomer concentration (M_b = 0.5 mol/L). (1) k_p = 1000 L/mol · s, r_c = 0.01 μm; (2) k_p = 60 L/mol · s, r_c = 0.1 μm. $C_*(0) = 10^{-5}$ mol/g-cat, $t_{1/2}$ = 3 hours.

comparable to Montedison catalyst and one of activity comparable to Stauffer AA in slurry. Because the intraparticle diffusion resistance decreases with time, its effect is much easier to detect in the yield at 0.5 hours. From Figure 8 for the low activity catalyst, the effect on the three hour yield would be difficult to detect if $D_\ell > \sim 2 \times 10^{-6}$ cm^2/s, but the difference in 0.5-hour yield at this diffusivity value would be as much as 20%. At $D_\ell = 1 \times 10^{-6}$, intraparticle diffusion resistance should be detectable in the three-hour yield. For high activity catalyst, when $M_b = 4$ mol/L, a significant difference in three-hour yield from 20 and 100 μm particles should be observable at $D_\ell \sim 10^{-5}$ cm^2/s, and a very large effect of particle size should be observed at 1/10th of this value. The effect of particle size on the 0.5-hour yield is still more significant. However, it is also important to note that as $D_\ell \rightarrow 0$, the polymerization will take place only at the surface of the catalyst particle. Thus, in the low-D_ℓ limit, it would be expected that the yield ratio would approach the ratio of surface areas or $(100/20)^2 = 25$, and this yield ratio would be independent of the polymerization time. However, this occurs at diffusivities well below the lower probable bound for D_ℓ of 10^{-6} cm^2/s. Comparison of Figures 8 and 9 shows that at low monomer concentration, the effect of particle size is more pronounced than at high M_b, as would be expected from the discussion of the previous section. Thus, under laboratory conditions, particle size effects could be detected at D_ℓ as high as 5×10^{-6} for low activity catalyst and $> 10^{-5}$ for high activity catalyst. It is pointed out that for very rapidly decaying catalysts, the disparity between the yield ratio at short and long times will be even greater than shown here. Figure 10 compares the rates observed over a high activity, second-order deactivating catalyst with particle sizes of 30, 60, and 90 μm. As the particle size is

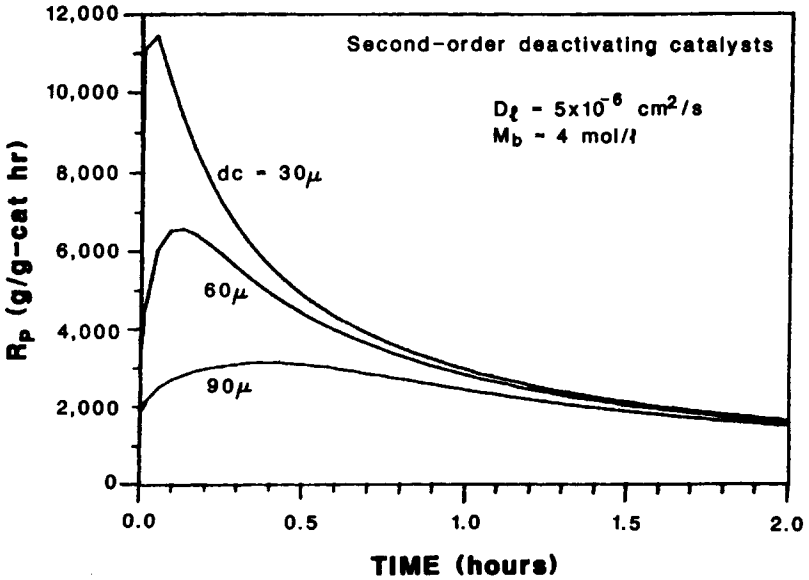

Fig. 10. Rate curves for polymerization over different particles sizes of high activity, second-order deactivating catalyst. $k_p = 2460$ L/mol · s, $C_*(0) = 10^{-5}$ mol/g-cat, $t_{1/2} = 0.25$ hours.

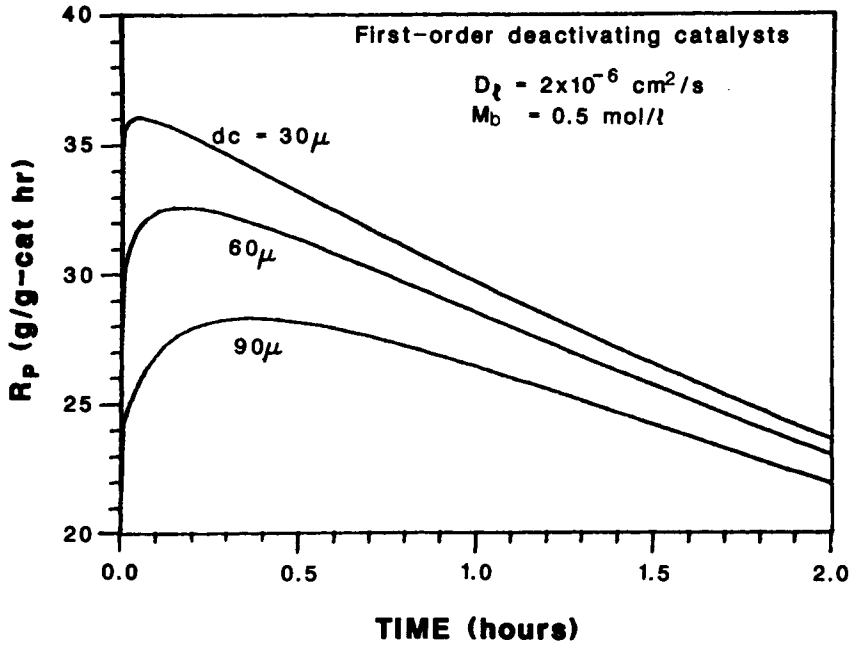

Fig. 11. Rate curves for polymerization over different particle sizes of low activity first-order deactivating catalyst. k_p = 100 L/mol · s, $C_*(0) = 0.5 \times 10^{-5}$ mol/g-cat, $t_{1/2}$ = 3 hours.

increased, the shape of the rate curve clearly goes from a decay type to a hybrid type.

Low activity catalysts are not necessarily immune to these effects. If the macroparticle diffusivity is sufficiently low, a catalyst of comparable activity to Stauffer AA may experience significant diffusion resistance under laboratory conditions (i.e., at low monomer concentration). Figure 11 illustrates the effect of catalyst particle size on the rate that would be anticipated for such a catalyst at a bulk monomer concentration of 0.5 mol/L, if $D_\ell = 2 \times 10^{-6}$ cm^2/s. From Figures 8 and 9 we see that for the low activity catalyst, the ratio of yields of 90 micron particles and 30 μm particles as a percentage is twice the value for M_b = 0.5 mol/L as when M_b = 4 mol/L. Thus, macrodiffusion effects are easier to detect under laboratory conditions than under industrial conditions. Experimentally, Tornqvist et al.[33] have observed a small effect of catalyst particle size (roughly 10% in the 1 hour yield) with a classical $TiCl_3$ catalyst in propylene slurry polymerization. The difference in reaction rate between the fractions was largest in the early stages of polymerization. Similarly, Schnecko et al.[34] observed that particles in the size range less than 47 μm were up to twice as active as those greater than 100 μm, in 20-minute polymerizations over a classical $TiCl_3$ catalyst. Also, the smallest catalyst particles produced the highest molecular weight polymer. Both Tornqvist et al.[33] and Schnecko et al.[34] showed that the specific surface was equivalent for all catalyst sizes. On the other hand, Reichert et al.[35] claimed no effect of catalyst particle size in polymerizations using a Hoechst catalyst.

It should be remembered that the large particle diffusivity is an effective diffusivity, and hence is proportional to the porosity. Hock[36] and Wristers[37]

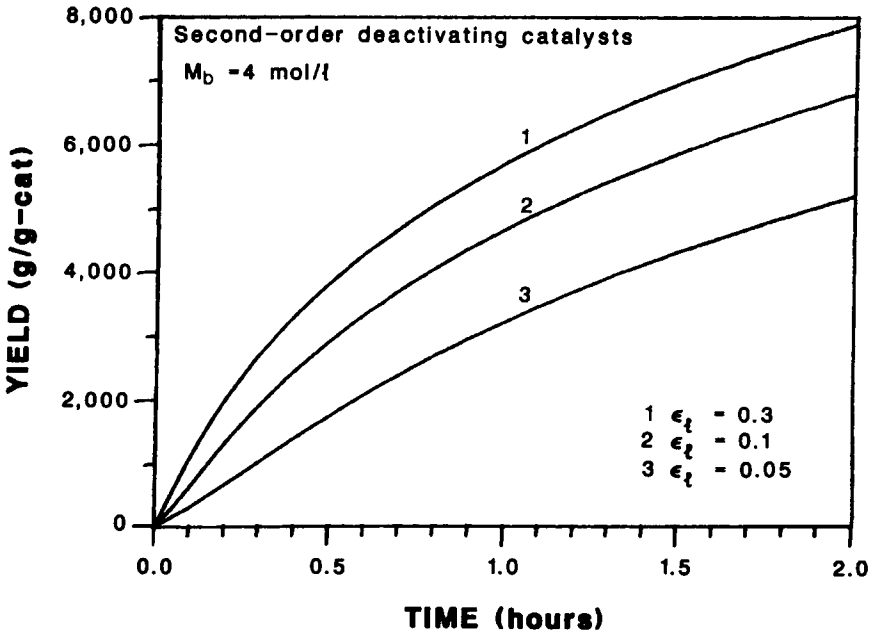

Fig. 12. Effect of macroparticle porosity on yield from high activity second-order deactivating catalyst. k_p = 2460 L/mol · s, $C_*(0) = 10^{-5}$ mol/g-cat, $t_{1/2}$ = 0.25 hours (1) $D_l = 5 \times 10^{-6}$ cm^2/s, Y_2 = 7880 g/g-cat. (2) $D_l = 1.67 \times 10^{-6}$ cm^2/s, Y_2 = 6780 g/g-cat. (3) $D_l = 0.83 \times 10^{-6}$ cm^2/s, Y_2 = 5190 g/g-cat.

have observed a correlation between the porosity of the catalyst and the polymer produced over it. Thus, the porosity of the catalyst may be expected to influence the diffusion resistance experienced in the polymerization. D_l would also be expected to depend on the amount of soluble polymer present in the liquid. Figure 12 illustrates that the macroparticle porosity may affect the catalyst productivity by 50% or more. If the catalyst porosity also affects the degree of breakup, still greater effects on the catalyst productivity might be anticipated. Numerous patents and articles, especially those related to ethylene polymerization over silica-supported catalysts, have stressed the importance of the porosity and pore size distribution of the support.[22,38-43] In particular, there appears to be a preference for average pore diameters in the range 100–600 Å, probably because pores smaller than 100 Å do not permit sufficiently rapid access to monomer for catalyst breakup. Soga et al.[44] presented a graph of productivity versus time for silica-supported catalysts with different pore sizes of the support. A pore diameter of around 200 Å was found to be necessary to achieve large productivities.

For unsupported catalysts, it seems reasonable that the number of active sites should be roughly proportional to the surface area. For this reason, ball milling of the catalyst, which decreases the primary crystallite size, has resulted in increased activities with these catalyst types.[29,33] The Solvay catalyst[45,46] represents a successful effort to prepare unsupported catalysts with high surface area and high porosity. For supported catalysts, high surface area of the support material is desirable, but not sufficient in itself for the achievement of high activity. Clearly, loading too much of the active

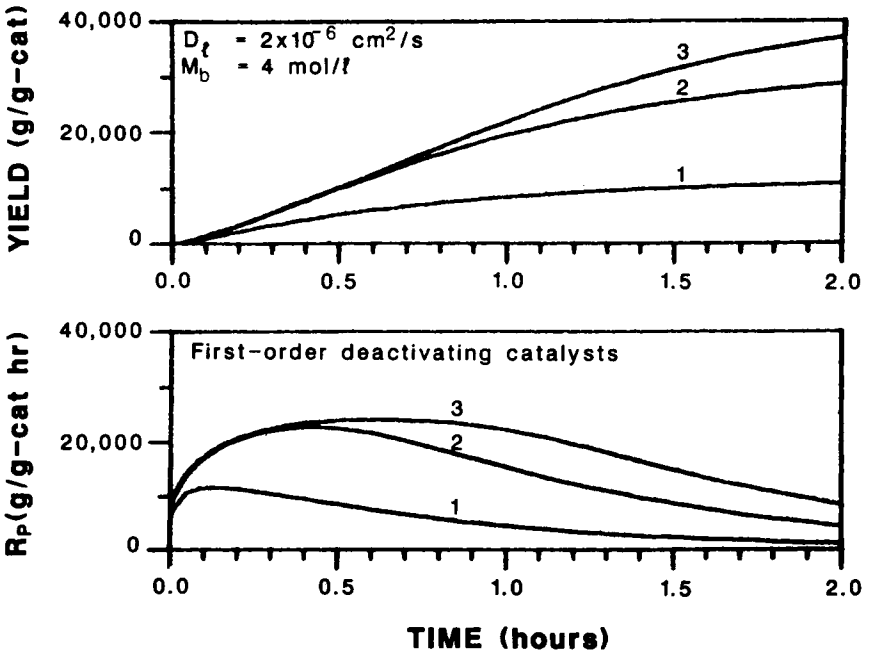

Fig. 13. Effect of active site loading on rate curves and catalyst productivity for high activity, first-order deactivating catalysts. (1) $C_*(0) = 10^{-5}$ mol/g-cat, Y_2 = 10,800 g/g-cat. (2) $C_*(0) = 4 \times 10^{-5}$ mol/g-cat, Y_2 = 28,600 g/g-cat. (3) $C_*(0) = 8 \times 10^{-5}$ mol/g-cat, Y_2 = 37,100 g/g-cat. All catalysts: k_p = 3100 L/mol · s, $t_{1/2}$ = 0.5 hours

component will result in its inefficient usage. Thus, various workers have observed that the yield per gram of transition metal decreased with loading, hyperbolically or even exponentially.[21,47-50] This may result from clustering, pore blockage or simply from the reaction becoming diffusion controlled. Baulin et al.[47] showed that during preparation of MgO-supported catalysts, both the pore volume and the average pore radius decreased significantly. In Figure 13, the onset of diffusion control with increasing loading is illustrated, for a typical second-order deactivating catalyst. At $D_\ell = 2 \times 10^{-6}$ cm^2/s, it is difficult to increase the rate above roughly 20,000 g/g-cat.h without using the transition metal wastefully. This in turn implies a high level of metal residues in the polymer, which may be unacceptable. As seen in Figure 13, the shape of the rate curve can provide an indication of overloading. It is interesting to note that almost all catalysts employed today have site concentrations in the range 10^{-5}–10^{-4} mol/g-cat. With a propagation rate constant around 1000 L/mol · s, this range of site concentrations leads to productivities of roughly 2000–20,000 g/g-cat · h in the absence of deactivation. From the simulations shown here, it seems probable that a further increase of an order of magnitude in the site concentration could in fact lead to highly diffusion-limited polymerizations.

EFFECT OF TEMPERATURE

In this section, the effect of temperature on the polymerization rate behavior will be considered. With an activation energy for propagation of

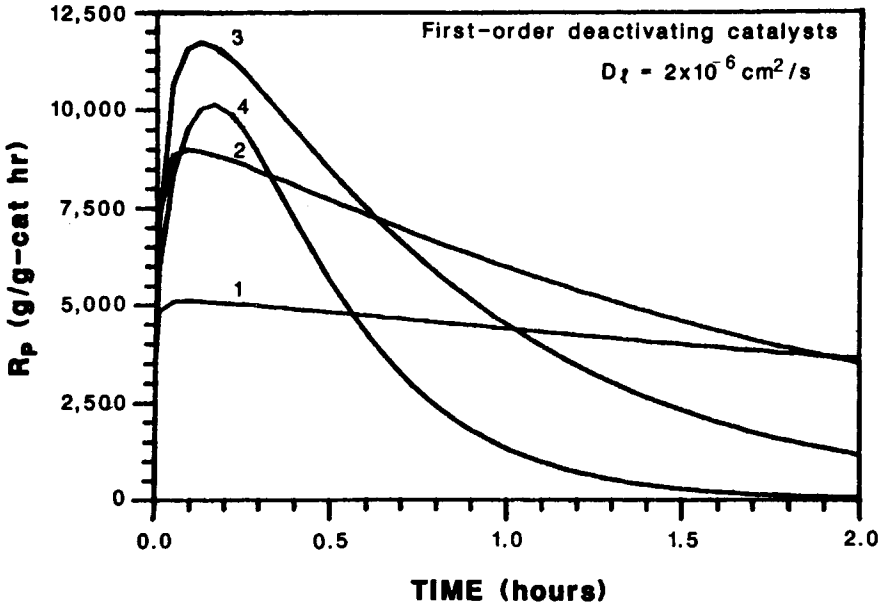

Fig. 14. Effect of temperature on polymerization rate at constant pressure ($P \sim 10$ atm). Propylene slurry polymerization over first-order deactivating catalyst, $C_*(0) = 10^{-5}$ mol/g-cat. $E_p = 10$ kcal/mol, $E_d = 10$ kcal/mol. 1 (30°C): $k_p = 453$ L/mol · s, $t_{1/2} = 3.4$ hours; 2 (50°C): $k_p = 1240$ L/mol · s, $t_{1/2} = 1.25$ hours; 3 (70°C): $k_p = 3100$ L/mol · s, $t_{1/2} = 0.5$ hours; 4 (90°C): $k_p = 6940$ L/mol · s, $t_{1/2} = 0.22$ hours.

10 kcal/mol, an increase or decrease in temperature of 20 K changes the propagation rate constant by a factor of around 2.5. If the polymerization is at all diffusion limited, these changes will clearly be sufficient to cause large changes in the degree of diffusion resistance experienced. To illustrate the type of behavior that is anticipated, Figure 14 shows representative simulations for polymerization over a high activity, first-order deactivating catalyst. The base case is assumed to be 70°C, and polymerization behavior at 30, 50, and 90°C is simulated, with a constant reaction pressure of 10 atm. The polymerizations at 70 and 90°C display the characteristics of a diffusion-limited deactivating system, while those at 30 and 50°C are essentially under kinetic control. For constant-pressure slurry polymerizations, the monomer concentration dissolved in the diluent will vary with temperature. The decrease in this monomer concentration driving force with increasing temperature also tends to enhance the diffusion resistance experienced over a fixed time, for reasons discussed above. Thus, in order to measure true activation energies, the best procedure is to adjust the reaction pressure to compensate for the change in monomer solubility in the slurry diluent. Many workers instead plot the rate of polymerization at constant pressure divided by the monomer concentration. With negligible mass transfer resistance, the Arrhenius plot for a nondeactivating catalyst will be a straight line, and the slope of the plot will yield the true activation energy for propagation. However, if the mass transfer resistance is significant, or if the catalyst deactivates, curvature in the Arrhenius plot may result, and the slope will yield an apparent activation energy which is different from the true value. To

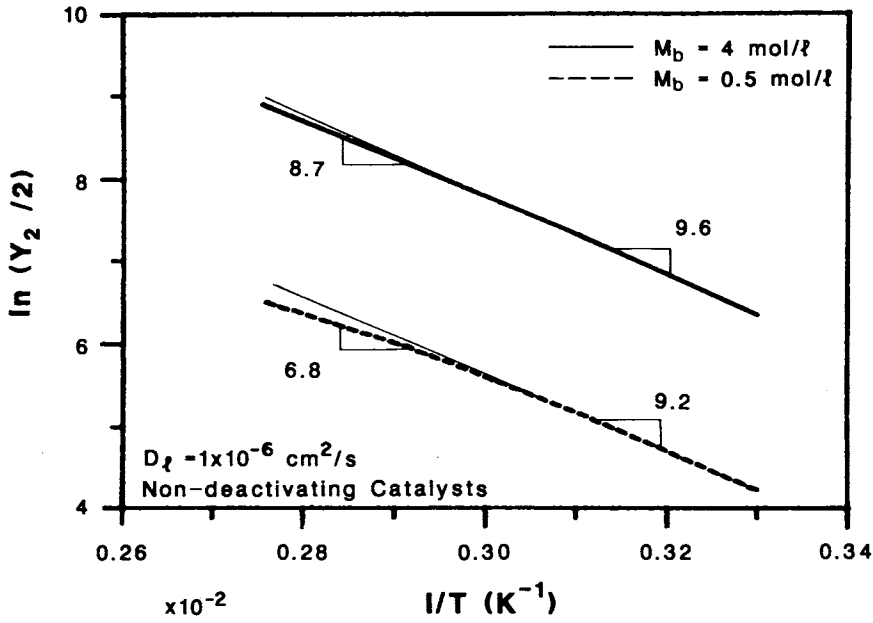

Fig. 15. Arrhenius plots for nondeactivating high activity catalyst at M_b = 4 mol/L and M_b = 0.5 mol/L. k_p at 70°C = 660 L/mol · s, $C_* = 10^{-5}$ mol/g-cat, E_p = 10 kcal/mol, E_d at 10 kcal/mol.

illustrate that intraparticle diffusion resistance can lead to curvature in the activation energy plot, Figure 15 shows data points for simulations for a nondeactivating high-activity catalyst, at 30, 50, 70 and 90°C and two different monomer concentrations. The true value of the activations energy for propagation was 10 kcal/mol. Although the lines appear quite straight, in the intervals 30–50 and 70–90°C, the observed activation energy changes from 9.6 kcal/mol to 8.7 kcal/mol for M_b = 4 mol/L, and from 9.2 kcal/mol to 6.8 kcal/mol for M_b = 0.5 mol/L. Thus, the apparent activation energy is considerably lower than the true value, especially at the low monomer concentration where mass transfer resistance is more significant. It is worthy of note that in the presence of mass transfer resistance, the Arrhenius plot based on the initial reaction rate should display more curvature than that based on the long time yields, and should give low values of the activation energy.[6] This is because the diffusion limitations are most severe during the initial stages of particle growth, as discussed previously. In the case of deactivating catalysts, a plausible alternative explanation for curvature in the activation energy plot is that of activated catalyst decay.[6,51] Figure 16 demonstrates Arrhenius plots for a high activity, first-order decaying catalyst, based on the average rate of reaction over a two-hour period. As before, the activation energy for propagation was 10 kcal/mol, and the activation energy of the first-order decay constant was varied from 5 to 20 kcal/mol. Although the physical properties are for slurry polymerization, negligible intraparticle mass transfer resistance was assumed in the simulations for this figure. It is seen that when E_d is 20 kcal/mol, a maximum in the Arrhenius plot is observed. Brockmeier[52] has reported an activation energy for the half-life of Montedison catalyst of 14.7

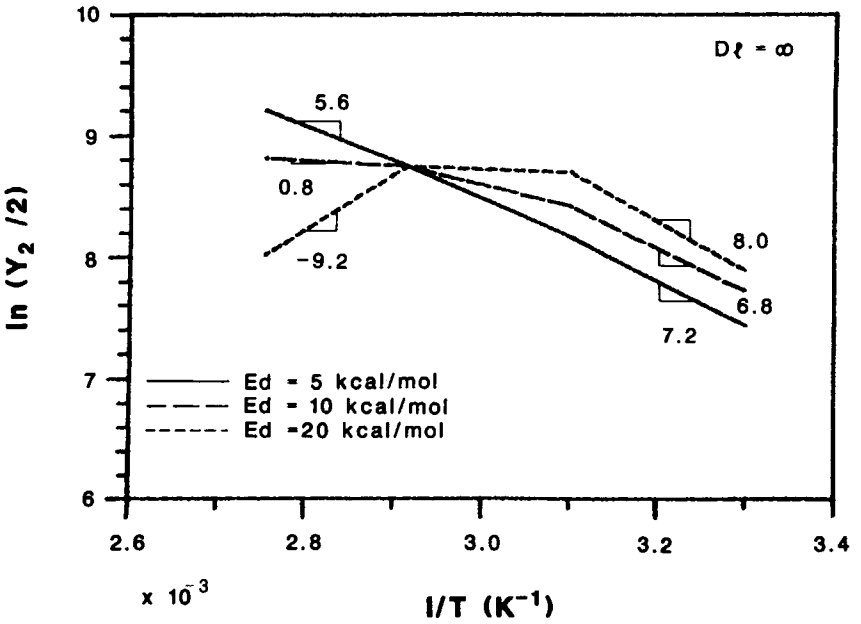

Fig. 16. Arrhenius plots for high activity, first-order deactivating catalysts with different activation energies for the decay constant. $M_b = 4$ mol/L, k_p at 70°C = 3100 L/mol · s, $C_* = 10^{-5}$ mol/g-cat, $t_{1/2} = 0.5$ hours, $E_p = 10$ kcal/mol.

kcal/mol (the activation energy for propagation was 15.6 kcal/mol). Munoz-Escalona and Parada[53] showed that catalyst decay was activated, but reported a relatively low activation energy of 3.5 kcal/mol. Keii et al.[21] and Munoz-Escalona and Parada[53] have observed a maxium in the Arrhenius plot in slurry polymerizations, while Zakharov et al.[27] observed a change in slope, corresponding to an activation energy change of 10 kcal/mol to 3 kcal/mol, for ethylene polymerization over a supported catalyst. In gas phase, Keii et al.[20] have observed a maximum in the Arrhenius plot for polymerization of propylene over a supported titanium catalyst, while Choi and Ray[19] observed curvature for propylene polymerization over Stauffer AA catalyst. Note that Figure 15 was calculated with $D_\ell = 1 \times 10^{-6}$ cm^2/s, the probable lower bound on the diffusivity for slurry polymerization. Mann[6,51] has shown that when $D_\ell = 5 \times 10^{-6}$ cm^2/s, the curvature in the Arrhenius plot is negligible for a catalyst of activity comparable to those considered here. Furthermore, in gas phase polymerizations, such severe macrodiffusion resistance would be very improbable. Since severe reductions in the apparent activation energy have been reported for gas phase polymerization, activated catalyst decay would probably be the explanation of choice in most circumstances, especially where maxima in the Arrhenius plots have been observed. If diffusion resistances are insignificant and the initial rate were used in the Arrhenius plot, a straight line should result and the true activation energy should be obtained. Thus, plotting the initial rate provides a means for distinguishing between these explanations. Unfortunately, this requires extrapolation, and it is often difficult to obtain the initial rates accurately.

MOLECULAR WEIGHT AND MOLECULAR WEIGHT DISTRIBUTION

In this section, the behavior of the molecular weight and molecular weight distribution (MWD) during polymerization will be considered. As discussed previously, the number and weight average molecular weight and the polydispersity may be obtained from ratios between the zeroth, first and second moments. For a system in which all concentrations and rate constants are constant, the limiting number average degree of polymerization at a given catalyst site is given by

$$\bar{\nu}_n^k = \frac{k_p^k M_c}{k_M^k M_c + k_A^k A^{1/2} + k_H^k H^{1/2}} = \frac{\alpha_k}{1 - \alpha_k} \tag{42}$$

During the initial stages of polymerization, the live polymer accounts for a significant fraction of the total. During this period, live chain growth is observed and the chain length gradually increases to the value given by Eq. (42). The mean chain lifetime at site k is given by

$$\tau_m^k = \frac{\bar{\nu}_n^k}{k_p^k M_c} = \frac{1}{k_M^k M_c + k_A^k A^{1/2} + k_H^k H^{1/2}} \tag{43}$$

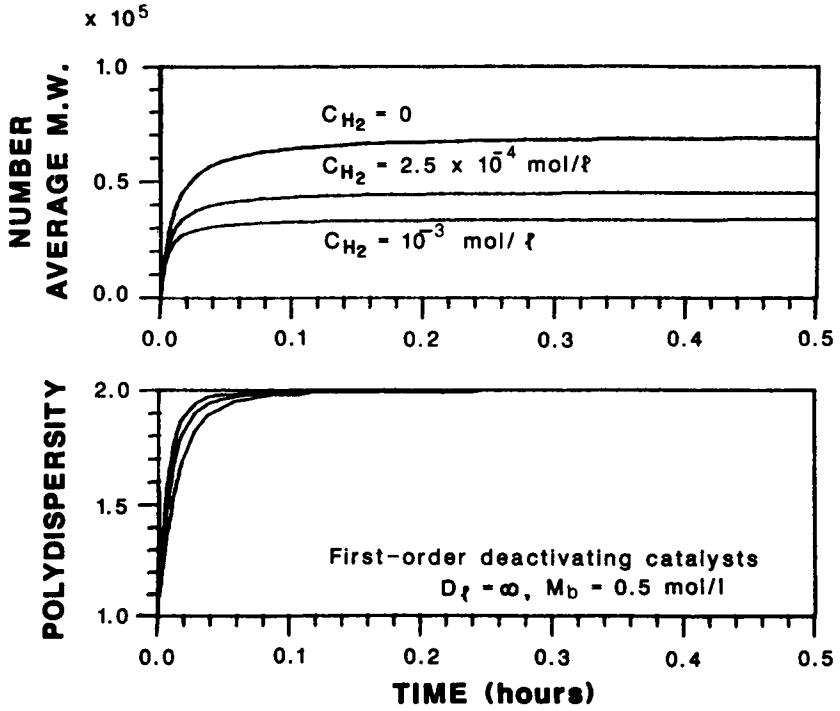

Fig. 17. Number average MW and polydispersity as a function of time and concentration of chain transfer agent. First-order deactivating catalyst, k_p = 100 L/mol · s, $C_*(0) = 0.5 \times 10^{-5}$ mol/g-cat, $t_{1/2}$ = 3 hours.

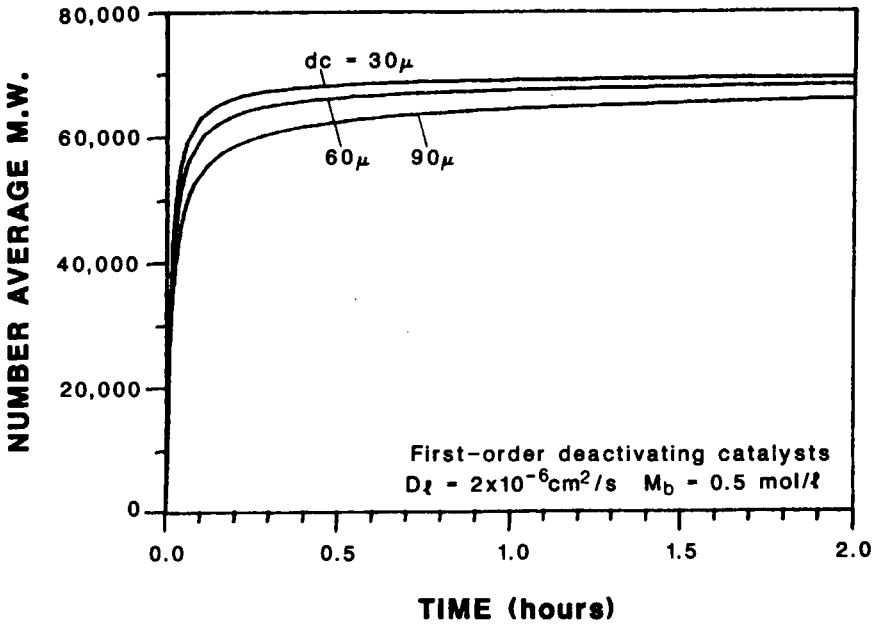

Fig. 18. Effect of intraparticle diffusion resistance on number average MW for 30, 60 and 90 μm particles of first-order deactivating catalyst. k_p = 100 L/mol · s, $C_*(0) = 0.5 \times 10^{-5}$ mol/g-cat, $t_{1/2}$ = 3 hours.

Thus, the mean chain lifetime is inversely proportional to the total chain transfer rate. From the work of Grieveson,[54] Zakharov et al.[55,56] and Baulin et al.,[30] it may inferred that for many polymerizations, the transfer rate constants for hydrogen and monomer or aluminum alkyl are approximately two and four orders of magnitude, respectively, smaller than the propagation rate constant, while spontaneous transfer is practically negligible. However, for some ethylene polymerizations, the propagation rate constant is very high relative to the chain transfer rate constants,[30,49] resulting in very high molecular weight polyethylenes. The time period for live chain growth is illustrated in Figure 17 for a low activity catalyst, where no large particle diffusion resistance and only one catalytic site was assumed. Note that the time constant for chain growth is larger in the absence of hydrogen (low transfer rate). During the period of live chain growth, the polydispersity gradually increases to 2, as predicted by the single-site kinetic mechanism. With many modern catalysts, the chain transfer rate is very rapid, resulting in almost constant molecular weight from very short times after the beginning of polymerization.[13,57,58] From the modelling equations above, one expects that intraparticle diffusion resistance should affect the molecular weight. This is illustrated in Figure 18, for different particle sizes of catalyst comparable to Stauffer AA under diffusion-limited conditions with a single catalyst site. These simulations were for the same catalyst as those of Figure 11, and it may be noted that the effect on molecular weight is much smaller than the effect on yield. The mean chain lifetime is roughly the same for all particle sizes, since hydrogen was the dominant chain transfer agent in this case and is not diffusion limited. For deactivating catalysts in the presence of severe diffusion

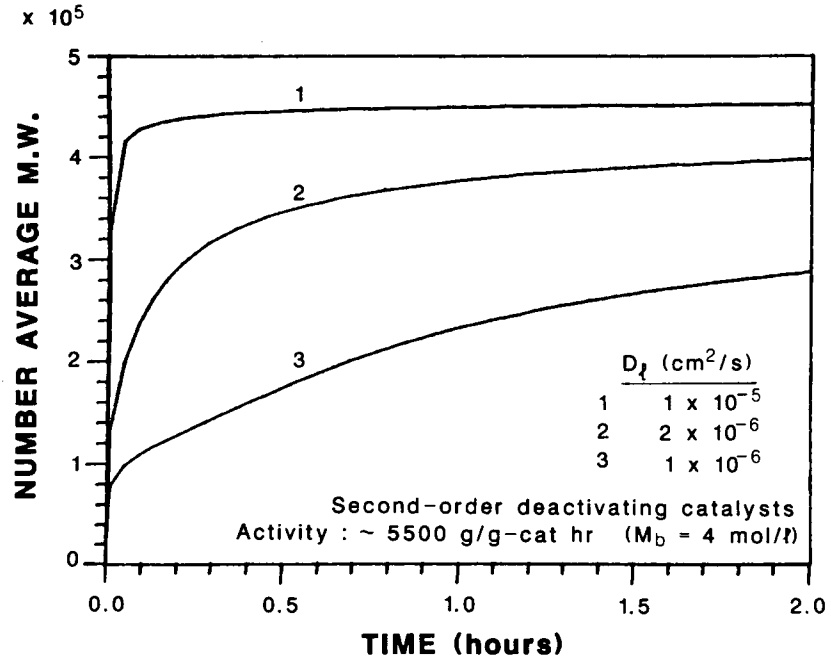

Fig. 19. Change in number average MW with time for second-order deactivating catalysts with varying degrees of macroparticle diffusion resistance. (1) k_p = 3600 L/mol · s, Y_2 = 11,700 g/g-cat; (2) k_p = 4200 L/mol · s, Y_2 = 11,600 g/g-cat; (3) k_p = 6600 L/mol · s, Y_2 = 11,800 g/g-cat. All catalysts: $C_*(0) = 10^{-5}$ mol/g-cat, $t_{1/2}$ = 0.25 hours.

limitations, an increase in the molecular weight with a time constant equivalent to the time constant for catalyst decay may be observed. This is because as the catalyst deactivates, the monomer concentration in the particle increases, hence the molecular weight continues to increase with time. This is illustrated in Figure 19 for second-order deactivating catalysts of average activity (over two hours) ~ 5500 g/g-cat.h.

One of the major mysteries in olefin polymerization over solid catalysts has been the reason for the broad molecular weight distribution that is commonly observed. While the maximum polydispersity predicted from a standard kinetic mechanism involving only propagation and chain transfer is $Q = 2$, in practice values of 5–10 for polypropylene and 10–20 for polyethylene are not uncommon.[59] There has been much speculation[1,60–64] as to whether intraparticle diffusion resistance might not be responsible for these broad MWDs. In the presence of severe diffusion resistance, the outer regions of the growing polymer particle see a much higher concentration of monomer than do the inner regions. Thus, according to the hypothesis, sufficient amounts of polymer of different molecular weights are produced to give a broad MWD. However, using realistic parameters in the Multigrain Model with a single type of active site, it was found that large polydispersities can only exist in the initial stages of polymerization. If the macroparticle diffusivity is greater than around 5×10^{-6} cm^2/s, the polydispersity after two hours' polymerization is less than 3 for catalysts of mean activity comparable to Montedison catalyst, despite initial activities as high as 20,000 g/g-cat/hr. The polydis-

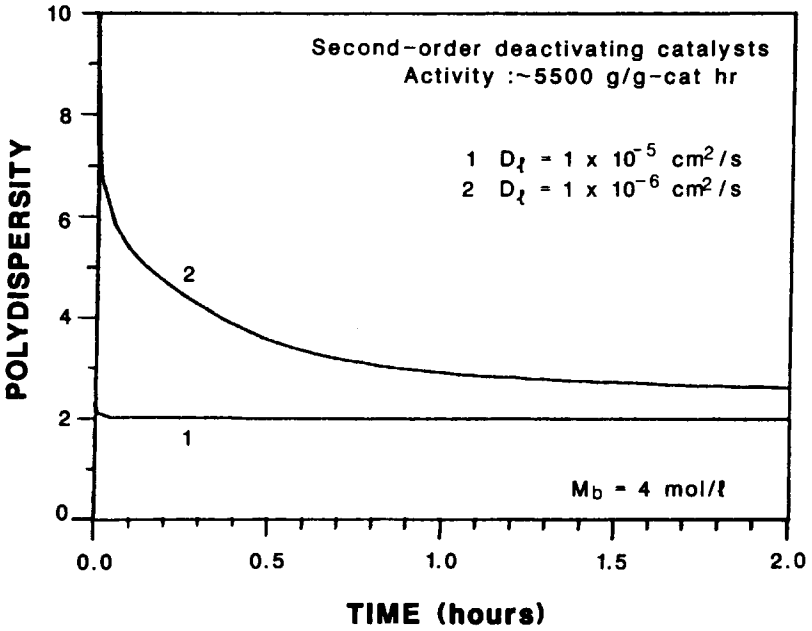

Fig. 20. Effect of intraparticle diffusion resistance on polydispersity for one-site catalysts. Second-order deactivating catalysts, $C_*(0) = 10^{-5}$ mol/g-cat, $t_{1/2} = 0.25$ hours. (1) $k_p = 3600$ L/mol · s, $Y_2 = 11{,}700$ g/g-cat; (2) $k_p = 6600$ L/mol · s, $Y_2 = 11{,}800$ g/g-cat.

persity that can result from intraparticle diffusion resistance is illustrated in Figure 20. It should be noted that even in this highly diffusion-limited situation, the polydispersity drops below 4 within 30 min. Clearly, with realistic diffusivity values, macroparticle concentration gradients alone cannot explain the breadth of the MWD at typical reactor residence times. Some experimental evidence which supports this viewpoint is the observation that with Phillips-type catalysts, the polymer MWD is very broad even under polymer-soluble conditions.[65] Furthermore, gas phase polymerizations, where $D_t \geq 10^{-4}$ cm^2/s, also show broad MWDs and these clearly cannot be explained by macroparticle diffusion. Thus, an alternative explanation to diffusion resistance must be sought. The other hypothesis to explain the broad MWD of olefin polymers which has received strong support is that of site heterogeneity. According to this idea, there exist sites of sufficiently varied activities and/or transfer rates that polymer of broad MWD is produced. It is pointed out that a "most probable" distribution of propagation or transfer rate constants (or, equivalently, diffusivities) cannot result in large polydispersity. However, employing an exponential surface distribution function of the form

$$f(\rho) = a\rho^{-b}(\rho_1 \leq \rho \leq \rho_2) \tag{44}$$

Keii et al.[13] were able to predict polydispersities as high as 9. On the other hand, examination of the primary crystal structure of unsupported catalysts indicates that various *distinct* types of sites may exist.[44,66] Apart from experimental evidence for the existence of isotactic and atactic sites in

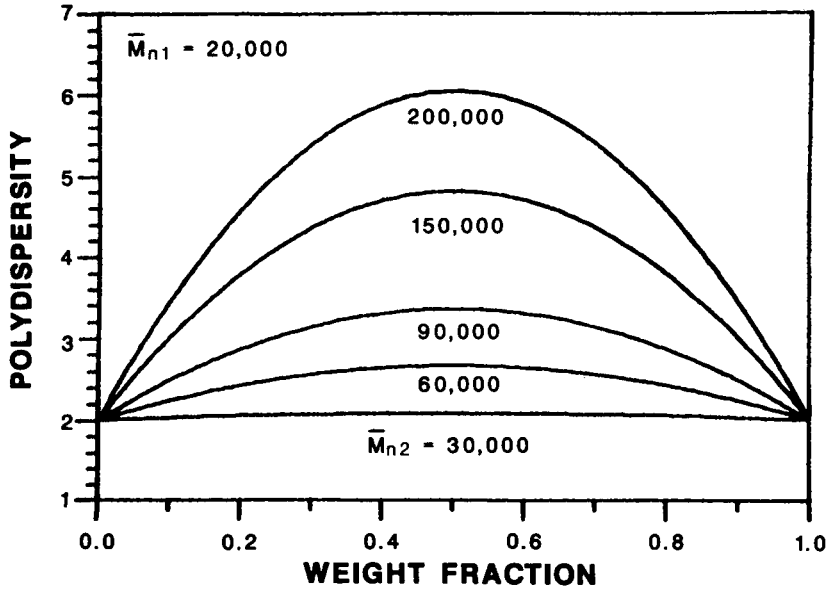

Fig. 21. Polydispersity resulting from combination of two polymer fractions, each with $Q = 2$.

propylene polymerization,[22,57,67] strong evidence for the presence of more than one type of active site in classical $TiCl_3$ catalysts (including Stauffer) has appeared recently.[68]

To model these effects we shall make use of the multisite multigrain model equations developed above. To illustrate the effects of multiple sites without the complication of intraparticle diffusion, let us consider a simple two-site model with each site producing polymer with the most probable distribution ($Q^1 = 2, Q^2 = 2$). Figure 21 demonstrates the overall MWD broadening that can arise from mixtures of two sites which produce different molecular weight polymer. This figure illustrates two important points:* (1) To achieve realistically broad polydispersities ($Q > 5$), the molecular weights produced by the two sites must differ by at least an order of magnitude. (2) In the case where the polydispersity of the individual sites are equal, the overall polydispersity is always at a maximum when each site contributes 50% of the total weight of polymer.

A third essential point may be seen by considering the case where each site produces polymer with equal polydispersities, i.e.,

$$Q^k = M_w^k/M_n^k = Q_f \qquad k = 1,2,\ldots,N \tag{45}$$

Noting that $M_w^k = Q_f M_n^k$, Eq. (18) may be rewritten as

$$Q = Q_f\left(\sum_{k=1}^{N} w_k M_n^k\right)\left(\sum_{k=1}^{N} w_k/M_n^k\right) \tag{46}$$

Thus, if intraparticle diffusion resistance (or other effects) cause the MWD at

*After completion of this work, we become aware of similar conclusions reported by E.G.M. Tornquist in Confidential Exxon reports in 1963.

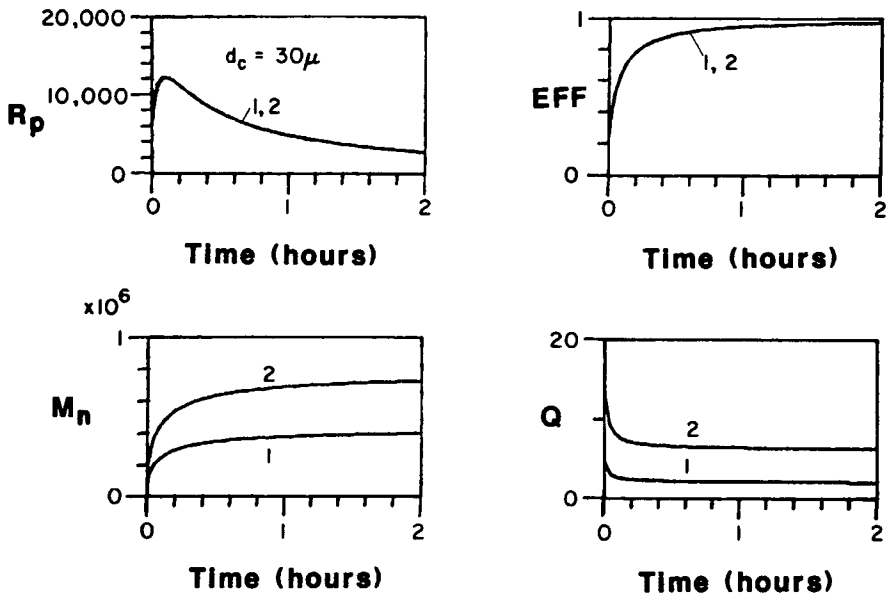

Fig. 22. Effect of diffusion resistance and site heterogeneity on polymerization rate, effectiveness factor, MW and polydispersity. High activity second-order deactivating catalysts with $d_c = 30$ μm, $D_\ell = 2 \times 10^{-6}$ cm^2/s. (1) Single-site catalyst, $k_p = 4200$ L/mol · s, $C_*(0) = 10^{-5}$ mol/g-cat, $t_{1/2} = 0.25$ hours. (2) Two-site catalyst, $k_p^1 = 4200$ L/mol · s, $C_*^1(0) = 0.5 \times 10^{-5}$ mol/g-cat, $k_p^2 = 4200$ L/mol · s, $C_*^2(0) = 0.05 \times 10^{-5}$ mol/g-cat, $M = 4$ mol/L, $t_{1/2}^1 = t_{1/2}^2 = 0.25$ hours.

the individual sites to be broader than $Q^k = 2$, then the overall distribution will be broadened in proportion. For example, if two sites of $Q^k = Q_f = 3.0$ are considered, the overall distribution will have a polydispersity 50% larger than for a combination of sites where $Q^k = Q_f = 2.0$. Thus, intraparticle diffusion resistance can *contribute* to MWD broadening, especially at relatively short times.

Figures 22–24 illustrate the combined effects of site heterogeneity and diffusion resistance (as a function of catalyst particle size) on the polymerization rate behavior and polymer properties for a high activity, second-order deactivating catalyst. The intrinsic average activity of this catalyst was roughly 7000 g/g-cat · h for a two-hour reaction time. In these simulations D_ℓ was chosen as 2×10^{-6} cm^2/s, a relatively low value. Figures 22 to 24 and are for 30, 60, and 90 μm particles of catalyst, respectively, and in each figure Curve 1 represents a single-site catalyst while Curve 2 represents a two-site catalyst in which the two sites decay in the same manner. Note that for the two-site catalyst, approximately 10% of the total sites are high activity and 90% low activity; however, the total activity is always equal to the activity of the catalyst of Curve 1. Hydrogen was assumed to be present, and the chain transfer rate constant for hydrogen was assumed to be 1/100th of the propagation rate constant of the catalyst in Curve 1 (all kinetic parameters were the same for all particle sizes).

From Figure 22 it is seen that for 30 μm particles diffusion resistance is mild, with the effectiveness factor reaching 0.9 after about 0.5 hours. For this case, a relatively normal decay-type rate curve is observed, and for the single site catalyst, the polydispersity is less than 3 after only 3 min, while the

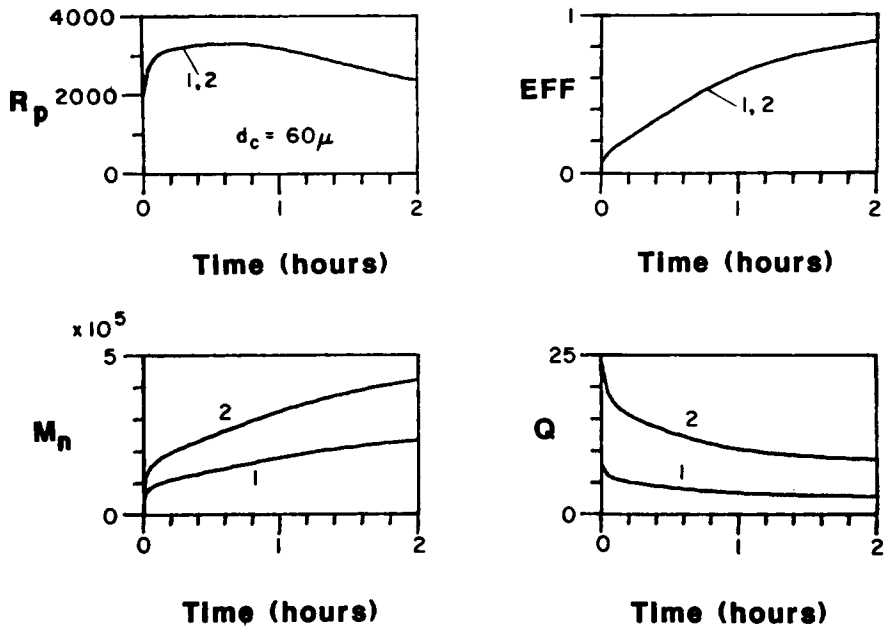

Fig. 23. Effect of diffusion resistance and site heterogeneity on polymerization rate, effectiveness factor, MW and polydispersity. High activity second-order deactivating catalysts with $d_c = 60$ μm, $D_\ell = 2 \times 10^{-6}$ cm^2/s. (1) Single-site catalyst, $k_p = 4200$ L/mol · s, $C_*(0) = 10^{-5}$ mol/g-cat, $t_{1/2} = 0.25$ hours. (2) Two-site catalyst, $k_p^1 = 4200$ L/mol · s, $C_*^1(0) = 0.5 \times 10^{-5}$ mol/g-cat, $k_p^2 = 42{,}000$ L/mol · s, $C_*^2(0) = 0.05 \times 10^{-5}$ mol/g-cat, $t_{1/2}^1 = t_{1/2}^2 = 0.25$ hours.

two-hour polydispersity is 2.11. For the two-site catalyst, on the other hand, the polydispersity after two hours is 6.4.

For the 60 μm catalyst particles, the rate curve turns into a broad hybrid shape, as seen in Figure 23. For this case, the effectiveness factor increases very slowly with time, and is equal to 0.83 even after two hours when the catalyst's intrinsic activity has died away considerably. The molecular weight shows a gradual increase characteristic of a strongly diffusion-limited system with a deactivating catalyst. For the single site catalyst, the polydispersity remains above 4 until $t = 0.6$ hours, while for the dual-site catalyst, the polydispersity starts from a very broad value of ~ 23 and decreases to around 9 after two hours.

Finally, Figure 24 shows the situation for the highly diffusion-limited 90 μm particles. In this case, an acceleration-type rate behavior is observed, and the effectiveness factor increases steadily with time. The two-hour yield from the 90 μm particles is 2370 g/g-cat, or only 20% of the yield from the 30 μm particles. The molecular weight increases steadily with time as does the effectiveness factor. In this extremely diffusion-limited case, the two-hour polydispersity from the single-site catalyst is 4.4 while for the dual-site catalyst it is ~ 13.

The factor of two difference in the MWD breadth for these different sized particles (even when there are two types of sites) is solely due to diffusion resistance. Thus for extremely large, high activity catalyst particles, significant MWD broadening could be contributed by macroparticle diffusion.

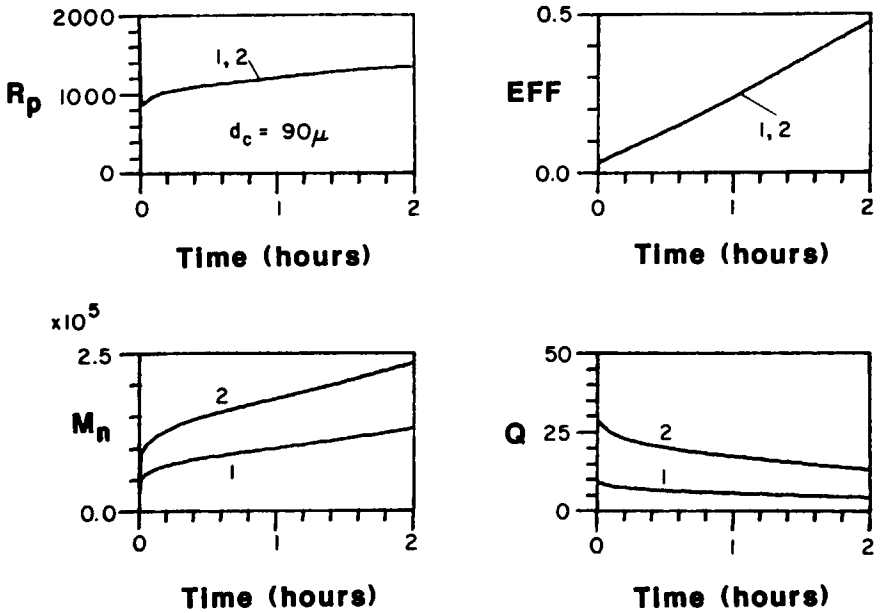

Fig. 24. Effect of diffusion resistance and site heterogeneity on polymerization rate, effectiveness factor, MW, and polydispersity. High activity second-order deactivating catalysts with $d_c = 90$ μm, $D_\ell = 2 \times 10^{-6}$ cm^2/s. (1) Single-site catalyst, $k_p = 4200$ L/mol · s, $C_*(0) = 10^{-5}$ mol/g-cat, $t_{1/2} = 0.25$ hours. (2) Two-site catalyst, $k_p^1 = 4200$ L/mol · s, $C_*^1(0) = 0.5 \times 10^{-5}$ mol/g-cat, $k_p^2 = 42{,}000$ L/mol · s, $C_*^2(0) = 0.05 \times 10^{-5}$ mol/g-cat, $t_{1/2}^1 = t_{1/2}^2 = 0.25$ hours.

It is possible to use these examples to examine whether or not a broad catalyst size distribution would have a significant effect on MWD broadening. By applying Eq. (18) for a mixture of two particles (rather than two sites) noting that $M_w^k = Q^k M_n^k$ for each particle we obtain

$$Q = \left(w_1 Q^1 + w_2 Q^2 \frac{M_n^2}{M_n^1} \right) \left(w_1 + w_2 \Big/ \left(\frac{M_n^2}{M_n^1} \right) \right) \tag{47}$$

Recall that for the 30 μm catalyst particle, $Q^1 = 2.11$ while for the 90 μm particle, $Q^2 = 4.4$. Also note that the ratio of number average molecular weights $M_n^2/M_n^1 \cong 1/3$. Thus assuming that we had a mixture of 30 μm and 90 μm catalyst particles and each catalyst size produced 50% of the total polymer, Eq. (47) predicts an overall polydispersity of 3.6, which is less than the polydispersity produced with the 90 μm catalyst particles alone. In addition, the large catalyst particles yield significantly less polymer than the small catalyst particles under the severe diffusion-limited conditions which produce broad polydispersity. Hence, the contribution of the large particles will be insufficient to cause MWD broadening, unless the particle size distribution is very strongly skewed towards the large particle sizes, a rather unlikely situation. For these reasons, it is likely that in general, little broadening is induced by the catalyst particle size distribution.

It is important to note that for catalysts with deactivating sites, the variation in the polydispersity with time is principally determined by the

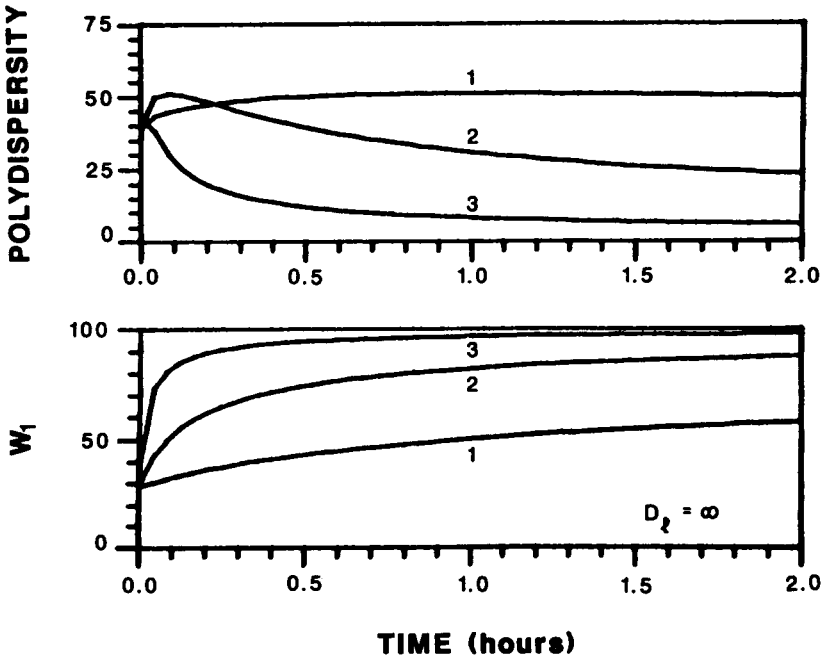

Fig. 25. Time dependence of the polydispersity for two-site catalysts and the weight fraction of polymer produced at Site 1. Site 1: $k_p^1 = 1000$ L/mol · s, $C_*^1(0) = 10^{-5}$ mol/g-cat, first-order decay, $t_{1/2}^1 = 3.5$ hours. Site 2: $k_p^2 = 10^5$ L/mol · s, $C_*^2(0) = 0.5 \times 10^{-6}$ mol/g-cat, second-order decay, 1: $t_{1/2}^2 = 0.1$ hours; 2: $t_{1/2}^2 = 0.01$ hours; 3: $t_{1/2}^2 = 0.001$ hours.

variation in the rate of decay of the two sites. If the weight fractions of polymer produced at each site start at close to 50% and gradually become imbalanced, the polydispersity will decrease with time. If the weight fractions are approaching 50%, the polydispersity will increase asymptotically with time. Of course, for some activity profiles of the sites, one will see a maximum in the polydispersity, which occurs when the weight fractions are exactly 50%. Examples of each case are illustrated in Figure 25 where Site 1 has a decay time constant of 3.5 hours while Site 2 has a decay constant of 0.1 hours (Curve 1), .01 hours (Curve 2) or .001 hours (Curve 3). Note that either increasing or decreasing polydispersity can arise depending on the relative rates of catalyst decay. From experiments described in the literature, various groups have reported that the polydispersity decreases asymptotically with time[60,69-73] or yield.[63] This is consistent with the decay of an active site which initially produces 50% or less of the total amount of polymer. The presence of a fast-decaying, highly active site with a propagation rate constant 40 times the average value was hypothesized by Bohm,[70] based on the molecular weight of polymer formed in the first few seconds of reaction. This very high molecular weight polymer did not increase with time. Crabtree et al.[63] also observed high molecular weight polymer formed after two minutes of polymerization, but attributed this to the absence of diffusion resistance due to encapsulation of the active sites at short reaction times. While reports of increasing polydispersity are rarer, Russian workers[74] reported a maximum in the polydispersity with time, and Taylor and Tung[75] have reported the

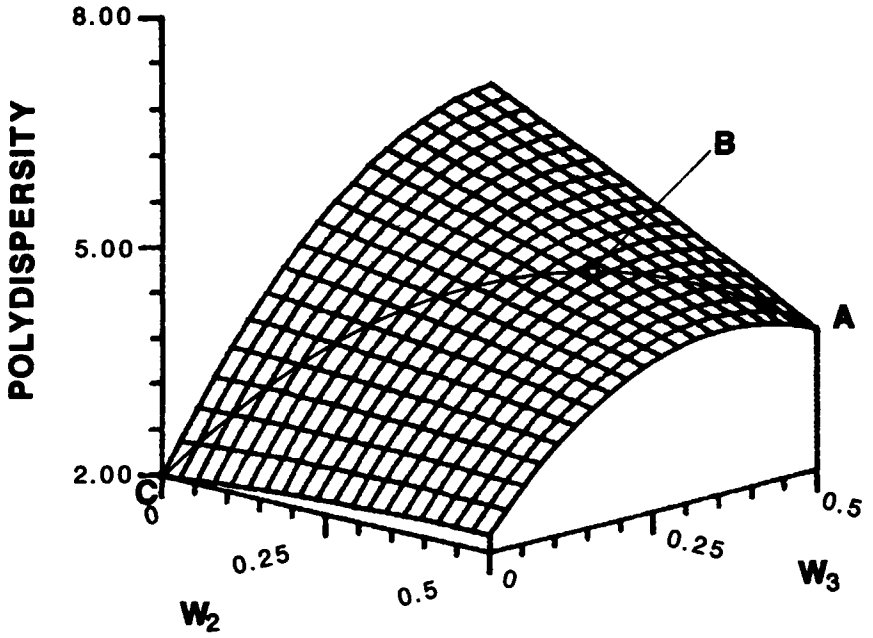

Fig. 26. Polydispersity resulting from combination of three fractions, each fraction with $Q = 2$. Relative activity of sites = 1 : 2 : 10.

polydispersity increasing with time over the first 30 minutes in low pressure slurry polymerization of ethylene. Keii et al.[57] showed that the polydispersity was almost constant for three hours of polymerization over a supported catalyst. A total polydispersity of around 5.5 resulted from combination of heptane-soluble and insoluble fractions of polydispersity around 3.[13,57] In perhaps the most convincing evidence of site heterogeneity to date, Rishina and Vizen,[68] employing carbon disulfide as a selective poison, showed that there are at least two types of sites in classical $TiCl_3$ catalysts including Stauffer AA. One site was highly active but unstable, and produced predominantly atactic polypropylene. They reported a total polydispersity of 11–13, while the polydispersities for individual fractions (soluble in various solvents) were as low as 2.5–3. Chien[69] reported that the polydispersity of amorphous PP produced over a $TiCl_3$ catalyst was less than three, and remained constant for up to 50 hours.

Similar analyses can be made for the case of three types of sites, etc. In particular, for three fractions with equal polydispersity ($Q_1 = Q_2 = Q_3 = 2$), Figures 26 and 27 illustrate the polydispersity obtained. The maximum polydispersity in Figure 26 is around 7 while that in Figure 27 is around 11. The most important point to recognize is that addition of more types of sites beyond two does not *necessarily* lead to further broadening. Broadening will result if the molecular weight being produced over the new type of site is either very large or very small, relative to the sites already present. However, a site that produces polymer between or close to that produced over the two sites already present may narrow the MWD. As an example, consider Point A on Figure 26. At Point A, Sites 2 and 3 are present, producing equal amounts

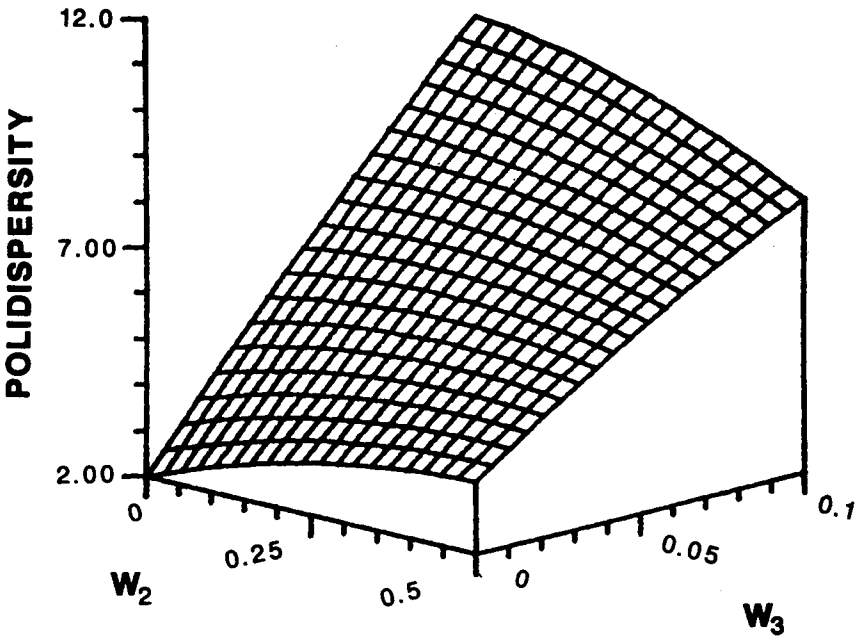

Fig. 27. Polydispersity resulting from combination of three fractions, each fraction with $Q = 2$. Relative activity of sites = 1 : 5 : 50.

of polymer to give a total polydispersity of around 4. On the line A-C, $w_2 = w_3$, so that this line represents the addition of a third site, Site 1, to an initial system with two sites producing equal amounts of polymer. The polydispersity increases to a maximum (point B), but falls thereafter. The most important general principle in analyzing the multisite cases is that roughly equivalent amounts of polymer of molecular weight differing by around one order of magnitude must be produced to result in broad MWD.

It is clear from the above discussion that no single trend in the polydispersity need exist for changes in reaction conditions. Variation in the monomer concentration, aluminum alkyl type and concentration, hydrogen concentration and temperature, etc. can lead to changes in the relative populations of active sites through deactivation and/or site formation. This has resulted in numerous contradictory effects of changes in these conditions, as reported in the comprehensive review by Zucchini and Cecchin.[64] However, it is likely that the generally broader polydispersities observed for polyethylenes, as compared to polypropylenes, may be due to the participation of more highly active sites in ethylene polymerization, as well as to increased diffusion resistance in the case of slurry polymerizations. Both these reasons are plausible, in view of the fact that ethylene polymerization rates are roughly two orders of magnitude higher than propylene polymerization rates, over comparable catalysts.[25,30,31,76]

Having shown that the presence of two or more types of sites can satisfactorily account for the magnitude of the polydispersity parameter, it is reasonable to ask whether the shape of the MWD curve can also be predicted. In the following figures, up to four "most-probable" distributions (corresponding to a

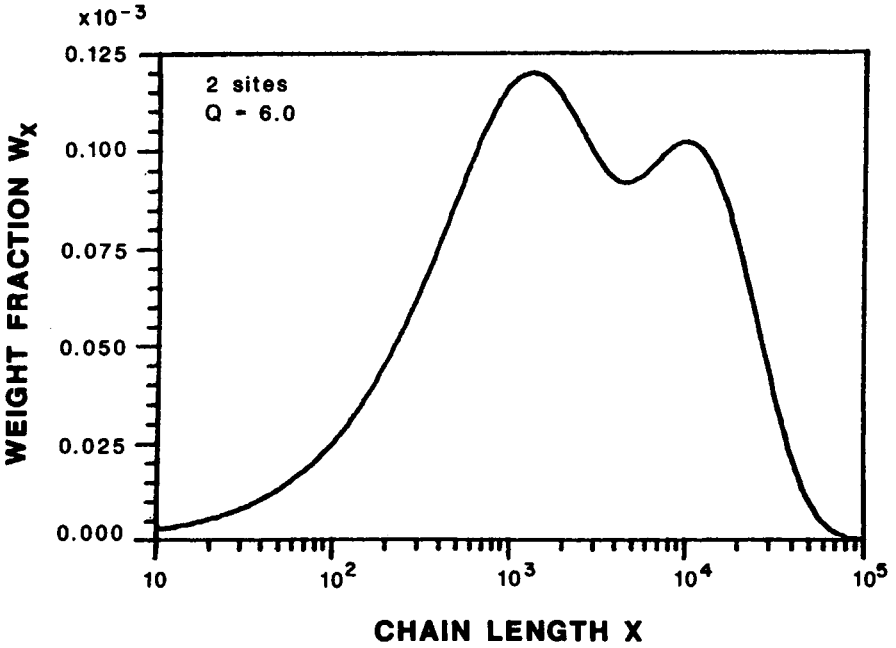

Fig. 28. Weight-MWD curve for combination of two polymer fractions with most probable distribution of chain lengths. $\nu_{n1} = 1000$, $\nu_{n2} = 10{,}000$, $w_1 = w_2 = 0.5$.

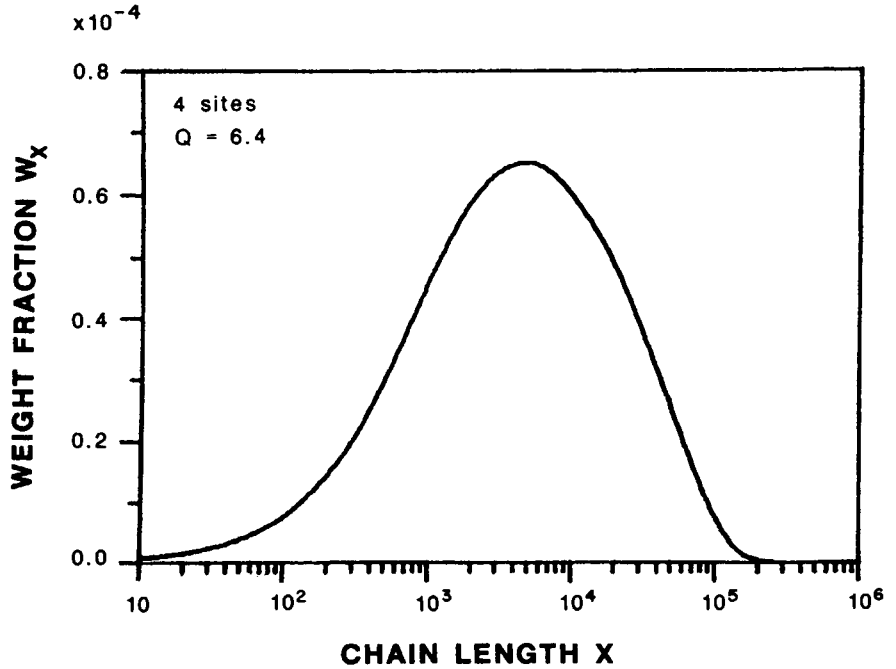

Fig. 29. Weight-MWD curve for combination of four polymer fractions with most-probable distribution of chain lengths. Ratio of chain lengths $\nu_{n1} : \nu_{n2} : \nu_{n3} : \nu_{n4} = 1 : 3 : 9 : 27$. Site fractions $\theta_1 = 0.519$, $\theta_2 = 0.333$, $\theta_3 = 0.111$, $\theta_4 = 0.037$. Weight fractions $w_1 = 0.148$, $w_2 = 0.284$, $w_3 = 0.284$, $w_4 = 0.284$.

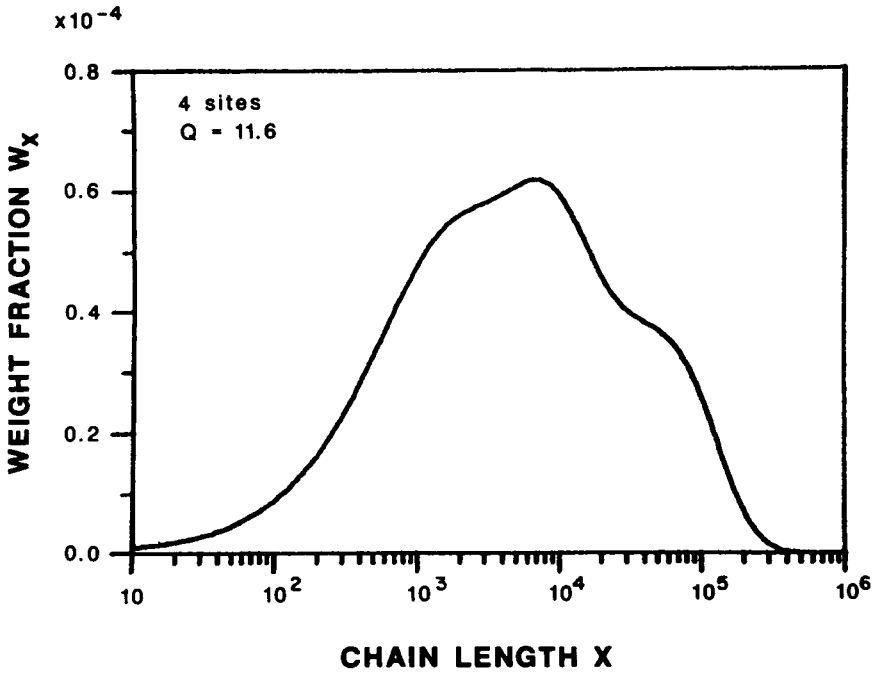

Fig. 30. Weight-MWD curve for combination of four polymer fractions with most probable distribution of chain lengths. Ratio of chain lengths $\nu_{n1} : \nu_{n2} : \nu_{n3} : \nu_{n4} = 1 : 5 : 10 : 50$. Site fractions $\theta_1 = 0.73$, $\theta_2 = 0.20$, $\theta_3 = 0.05$, $\theta_4 = 0.02$. Weight fractions $w_1 = 0.226$, $w_2 = 0.310$, $w_3 = 0.155$, $w_4 = 0.310$.

polydispersity of two for the polymer produced at each site) have been superimposed, according to their relative weight. Figure 28 shows a case where two types of sites, one of activity ten times that of the other, combine to form equal amounts of polymer. In this case, the weight-MWD curve which would be observed through permeation chromatography is bimodal, with a polydispersity of 6. Clearly, with only two types of sites it is difficult to predict smooth unimodal MWD curves—although mass transfer resistance of column dispersion effects which are present in experimental (GPC) gel permeation chromatography could smooth shoulders in the MWD to produce smooth unimodal chromatograms from MWDs such as shown in Figure 28. However, with a larger number of sites, broad unimodal MWD curves are readily generated. For example, Figure 29 illustrates that with four types of sites, producing roughly equal amounts of polymer, very smooth, realistic MWD curves are predicted. The polydispersity was 6.4 in this case, with the highest activity site possessing 27 times the activity of the lowest. Keii et al.[13] have presented MWD curves very similar to the one shown here, for polypropylenes produced over classical titanium trichloride catalysts. Figure 30 illustrates another four-site combination, but this time with a polydispersity of 11.6. The MWD curve is skewed, but with some GPC column dispersion this might not be as clearly evident as pictured here. For the Stauffer AA-DEAC system Rishina and Vizen[68] show a GPC curve with Q ≈ 12 which resembles this one. Finally, Figure 31 shows a peak with four sites and a total polydispersity of

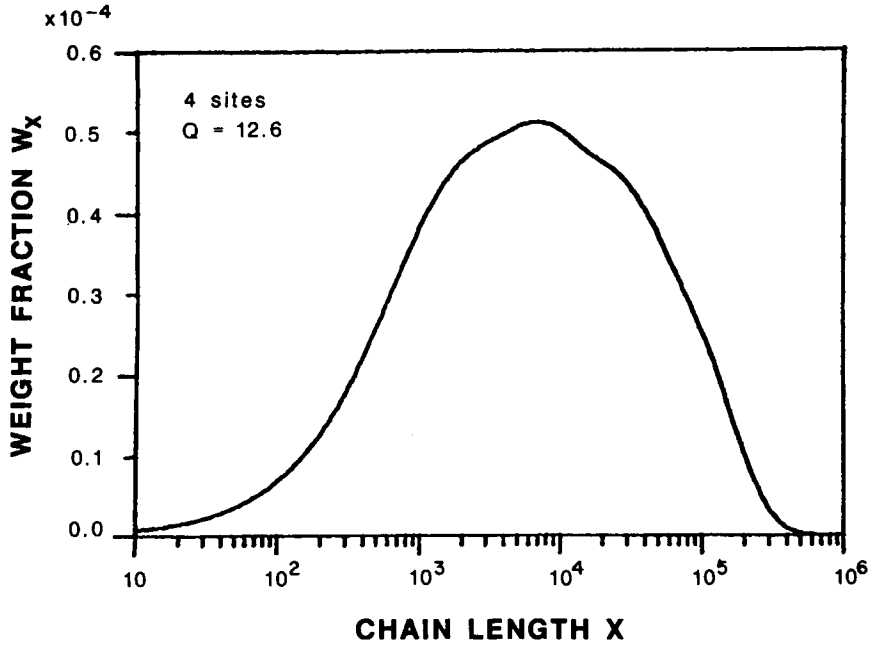

Fig. 31. Weight-MWD curve for combination of four polymer fractions with most probable distribution of chain lengths. Ratio of chain lengths $\nu_{n1} : \nu_{n2} : \nu_{n3} : \nu_{n4} = 1:4:16:64$. Site fractions $\theta_1 = 0.672$, $\theta_2 = 0.250$, $\theta_3 = 0.063$, $\theta_4 = 0.016$. Weight fractions $w_1 = 0.183$, $w_2 = 0.272$, $w_3 = 0.272$, $w_4 = 0.272$.

12.6. The presence of individual sites is completely indistinguishable in this case. In summary, one may conclude that with only two types of sites, GPC chromatograms for broad MWD samples would appear bimodal unless there was extensive column dispersion. However, with four distinct types of sites, smooth unimodal peaks can be obtained, as also found by Vizen and Yakobson.[73] However, even when only two types of sites are present, the multimodal character of the peaks may be masked by factors such as diffusion influence (broadening the peak for each individual site), a distribution of energies for each site type, and GPC column broadening. For application of these ideas to the copolymerization of olefins, see the work of Heiskanen.[14,77]

MWD CONTROL IN INDUSTRIAL CATALYSTS

From a practical standpoint, addition of a second or third type of active component to the catalyst has successfully resulted in MWD broadening in numerous cases. In one Japanese patent,[78] the polydispersity was more than doubled by using a combination of two components such as $TiCl_4$ and Ti(OPr)4. The ratios of these components for attaining the broadest MWD appeared to be around 3 : 1. Other patents[79-84] refer to the use of compounds of more than one transition metal. Combinations of zirconium or vanadium with titanium or chromium are particularly common. In one case,[82] it was noted that there was an optimum polymerization temperature for MWD broadening, which is consistent with the hypothesis advanced above, if one assumes that the different types of sites have different activation energies. In

another patent, the MWD was controlled solely through variations of Zr/Ti.[84] In general, it appears that zirconium compounds tend to increase the molecular weight, but are not very active. Hence, there is a tradeoff between MWD broadening using Zr and increased residues in the polymer. This is also true when another approach, that of deactivating additives, is employed. A Japanese patent[85] describes the use of additives which decreased the yield by 10–20% while *increasing* the polydispersity from 13 to 20 or more. From the previous section, it is clear that catalyst poisons need not always cause narrowing of the MWD. For example, in a two-site catalyst, if the added compound selectively poisons a site which produces a large percentage of the total polymer, a broadening of the MWD may result.

At other times, narrowing of the MWD is the goal. For this, certain supported catalysts have been found capable of producing polydispersities of less than 4.[13,50,86,87] With unsupported Ti-based catalysts, the value of the polydispersity generally ranges from around 9 to as high as 18,[13,50,68,76] while for single transition metal supported catalysts, values of polydispersity from 3 to 10 are commonly reported.[13,50,58,67,76] This may be due to relatively homogeneous deposition of the active component on the support, and is consistent with the site heterogeneity hypothesis of MWD broadening. In addition, the polydispersity clearly varied with the type of support, with magnesium-based supports giving the lowest polydispersities.[50] In all cases, the preparation conditions were found to be of critical importance for MWD control.[80,84,86,88] In view of the sensitivity to relative active site concentrations demonstrated in the previous section, this is not at all surprising. For single-transition metal catalysts, it is the degree of reduction which appears to be of paramount importance. In a Japanese patent,[85] reduction with TEA (triethylaluminum) was found to lead to a broader MWD than reduction with DEAC (diethylaluminum chloride), which is a less powerful reducing agent. TEA was also preferred over triisobutylaluminum as an activating agent in order to achieve MWD broadening.[83] In Ref. 50, it was determined that the titanium component was reduced less over magnesium-based supports than over other support materials. Thus, it appears that reduction leads to the formation of several types of active sites (probably based on different valence states of the transition metal) which can produce broad MWDs.

EFFECTS OF EXTERNAL FILM RESISTANCES

All of the simulations presented above included the effects of external film heat and mass transfer, using the Ranz-Marshall correlations[5] to evaluate the heat and mass transfer coefficients. For slurry polymerization, the particles were assumed to move relative to the fluid at their terminal velocity. This assumption would tend to overestimate the resistances in the external film.[5] Nevertheless, even for the high activity catalysts considered, the maximum temperature rise for 30 μm catalyst particles was under 5 K, and the maximum concentration drop was of the order of 5% of the bulk concentration. Although an intrinsic activity of 20,000 g/g-cat · h would suggest an initial temperature rise as high as 10 K in slurry polymerization, strong intraparticle diffusion resistance coupled with the very rapid increase in particle size in the early stages of growth combine to reduce the initial

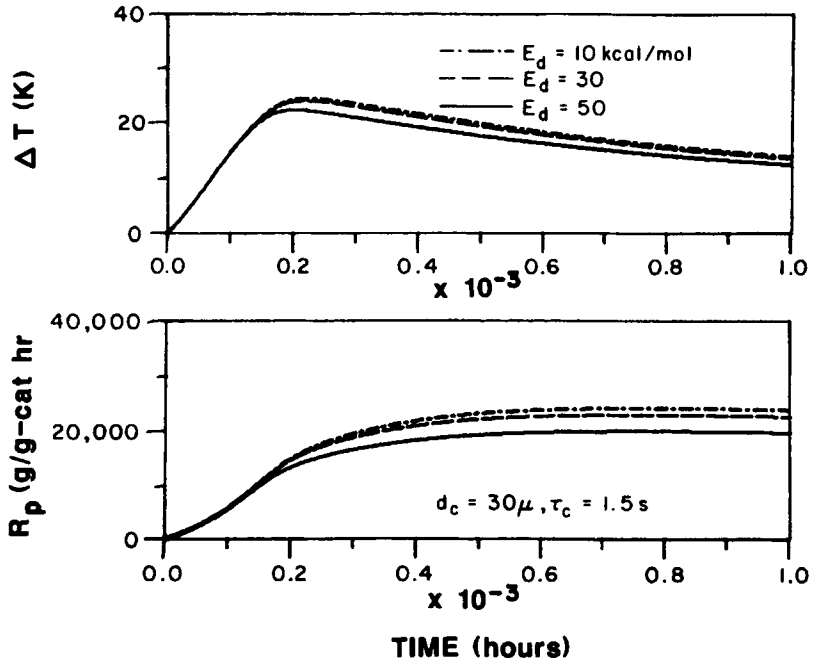

Fig. 32. Temperature profiles and polymerization rate at short times for high activity catalyst in gas phase propylene polymerization in a stirred bed reactor (u = 2 cm/s). $C_*(0) = 10^{-5}$ mol/g-cat, $t_{1/2}$ = 0.25 hours (isothermal conditions), M_b = 1 mol/L, E_p = 10 kcal/mol, E_d = 10, 30, 50 kcal/mol.

temperature rise by a factor of 2–4. Since the external film resistances decrease with the square of polymer radius, their effect is insignificant over the normal time scale for polymerization (minutes to hours).

In gas phase polymerization, on the other hand, initial temperature rises are frequently very large. This temperature rise may affect the subsequent course of the polymerization in various ways. If the activation energy for catalyst decay is less than or equal to that for propagation, the temperature rise will lead to an increase in the yield. However, if the activation energy for the decay is greater than that for propagation, the initial temperature rise may lead to a loss in productivity. This is illustrated in Figures 32 and 33 for 30 μm particles of second-order decaying catalyst with initial activity around 20,000 g/g-cat · h, and an activation energy for propagation of 10 kcal/mol. Figure 32 shows the external film temperature rise and the instantaneous rate for the first 3.6 seconds of polymerization. For this catalyst of high intrinsic activity, the temperature can reach the polymer melting point. Because the behavior when the melting point is reached is unpredictable, it was assumed that the catalytic sites become fully activated with a characteristic time of 1.5 s, which results in a maximum temperature rise of around 25 K. When the activation energy for the decay is very large (E_d = 50 kcal/mol), considerable deactivation takes place during this initial period, and the polymerization rate decreases. On going from E_d = 10 kcal/mol to 50 kcal/mol, Figure 33 shows that the catalyst productivity decreases by around 15%. It should be noted that a temperature rise of ~ 50 K changes the rate of decay by a factor of 40,

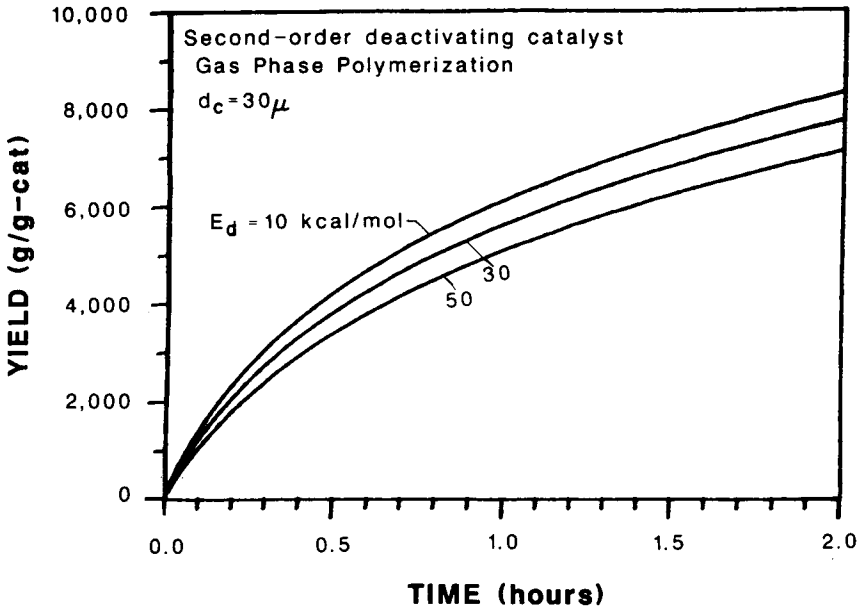

Fig. 33. Effect of activation energy for catalyst decay on productivity of high activity catalyst in gas phase propylene polymerization in a stirred bed reactor (u = 2 cm/s). Second-order deactivating catalyst, k_p = 10,000 L/mol · s, $C_*(0) = 10^{-5}$ mol/g-cat, $t_{1/2}$ = 0.25 hours (isothermal conditions), M_b = 1 mol/L, E_p = 10 kcal/mol, E_d = 10, 30, 50 kcal/mol.

when E_d = 20 kcal/mol, or a factor of 10,000, if E_d = 50 kcal/mol. Thus, for E_d = 50 kcal/mol, a temperature rise as high as 50 K, even for a period as short as a few seconds, catastrophic decay will result, and very large effects on the catalyst productivity may be expected.

In principle, similar effects to those shown in Figures 32 and 33 might exist in slurry polymerizations. However, due to the small temperature rise in slurry, the effects are predicted to be less severe, even for catalysts more active than those considered here. Only if there is rapid and irreversible transformation of active centers a few degrees above the reaction temperature could the temperature rise become a serious problem. In either gas or slurry, any problems caused by the initial temperature rise may be avoided by the methods discussed in Ref. 5 (e.g., prepolymerization at mild conditions).

It is also pertinent to consider the potential effect of the external film resistances on polymer properties. Earlier work with the multigrain model[3] has shown that even under the most extreme overheating conditions, there are only very short-term effects on the MWD. For example, in a simulation of 60 μm particles of a deactivating catalyst displaying an initial peak activity of 20,000 g/g-cat.h, the temperature in the particle reached the melting point of the polymer for a brief period of about a second. However, the maximum polydispersity was around 2.13, even in this case. In comparison to the case where external film resistances are neglected, particle overheating may increase the yield by as much as 10% and the molecular weight by 5%, but the polydispersity at two hours is only 2.04. The fact that such a small fraction of total polymer is produced in this initial overheating period means that the effect on polymer product properties is negligible.

In summary, it is safe to conclude that the external film resistances exert a negligible effect on both the rate behavior and polymer properties in slurry polymerization. In gas phase, the external film mass transfer resistance exerts a negligible effect; however, the large initial temperature rises observed with high activity catalysts of large particle size may be sufficient to increase the yield and molecular weight by several percent (assuming that the reaction is not stopped by encapsulation due to melting polymer). However, there is a negligible effect on MWD broadening.

DETECTION OF INTRAPARTICLE DIFFUSION RESISTANCE

In design of industrial catalysts, it is clearly desirable to be aware when intraparticle diffusion resistance is present. If intraparticle diffusion resistance is detected, catalyst properties may be optimized with substantial improvements in activity. If not detected, intraparticle diffusion resistance might result in elimination of otherwise promising catalyst systems from consideration. Knowledge of the diffusion resistance is also important in predicting the behavior of laboratory-tested catalysts under industrial conditions. Here, several methods for the detection of intraparticle diffusion resistance will be suggested. It is first pointed out that if sharply decaying rate curves such as Curve 1 in Figure 5 are observed, then it is virtually certain that the reaction has no significant macroparticle mass transfer effect. The first telltale sign of macroparticle diffusion resistance is thus an acceleration or hybrid-type rate curve. If such a rate curve is observed, the most unambiguous method for testing for macroparticle diffusion resistance is variation of the catalyst size. By carefully fractionating samples of catalyst and verifying that the transition metal loading is the same for each fraction, one tests the productivity of each fraction to determine whether diffusion resistance is indeed a factor. A weaker indicator of macroparticle diffusion resistance is nonlinearity in the polymerization rate (or yield for a fixed time) versus bulk monomer concentration. This presupposes the ability to estimate the monomer concentration with accuracy. Since the relation between the monomer concentration in slurry diluent and monomer pressure is nonlinear,[16] the rate should not be plotted versus pressure. Finally, a nonlinearity in the Arrhenius relation may also be indicative of diffusion resistance, at either the macroparticle or microparticle level if initial rates are used to construct the Arrhenius plot.

CONCLUSIONS

In this paper, the potential effects of intraparticle mass transfer and external film mass and heat transfer on polymerization behavior have been examined. Intraparticle diffusion resistance can manifest itself in a variety of ways, including the shape of the polymerization rate curve, catalyst particle size effects, nonlinearities in the rate vs. concentration, in Arrhenius plots, etc. At the levels of catalyst activities employed today, the degree of diffusion resistance experienced is strongly dependent on the physical properties of the catalyst. However, significant concentration gradients in the macroparticles can exist at short times (i.e., at low growth factor) in slurry polymerization, even for catalysts of relatively low activity. For large particles of high activity catalyst, intraparticle mass transfer resistance can be rate limiting over longer

periods. With diffusion-controlled reaction, acceleration or hybrid-type rate behavior will be observed. The rate limitation in these cases might result from mass transfer of cocatalyst (which is thought to participate in active site formation) as well as monomer, especially when catalyst and cocatalyst are not premixed. A test of the effect of catalyst particle size on yield may be performed to confirm the presence or absence of intraparticle diffusion resistance. In gas phase, macroparticle diffusivities are presumably high enough to avoid significant concentration gradients, although a low diffusivity during catalyst breakup is not inconceivable.

Diffusion resistance, where present, affects the polymerization rate more strongly than the polymer properties. In particular, it is unlikely that concentration gradients alone can account for the broad MWDs of olefin polymers observed in practice. The experimental evidence, from analysis of isotactic and atactic fractions and polymer produced over certain supported catalysts, also suggests that the maximum polydispersity produced over a single type of active site is around 3. A multiplicity of types of active sites, on the other hand, offers a convincing explanation both of the polydispersity and the shape of MWD curves that are observed by gel permeation chromatography. The polydispersity is at a maximum when the weights of polymer produced over sites with different characteristics are roughly equivalent. To attain broad MWDs, polymer fractions of molecular weight differing by roughly an order of magnitude should be present. The above insights can be used in tailoring the MWD produced over solid catalysts. In practice, the method of choice for MWD broadening is frequently the use of two or more active components based on different transition metals, while for MWD narrowing, the use of a support with a single active component is preferred. In either case, the preparation conditions, especially those related to the degree of reduction of the catalyst, are of paramount importance. Finally, the effects of external film heat and mass transfer are largely insignificant on the polymerization behavior and polymer properties on the time scale of a particle's residence in an industrial reactor. However, the short time large temperature rises encountered with high activity catalysts in gas phase polymerization may affect the polymerization in ways that are hard to predict, due to softening and melting of the polymer.

LIST OF SYMBOLS

A	Concentration of organoaluminum compound
c	Dimensionless monomer concentration
C_*, C_*^k	Concentration of active sites [mol-sites/ℓ-cat]
C_p	Heat capacity of polymer
d_c	Diameter of catalyst particle
d_p	Diameter of polymer particle
D_b	Bulk diffusivity of monomer
D_l	Effective diffusivity in macroparticle
D_s	Effective diffusivity in microparticle
E_d	Activation energy for catalyst decay constant [cal/mol]
E_p	Activation energy for propagation [cal/mol]
H	Concentration of hydrogen
ΔH_p	Heat of polymerization [cal/mol]
k_A, k_A^k	OAC chain transfer rate constant

k_e	Effective thermal conductivity in polymer particle [cal/cm · s · k]
k_f	Thermal conductivity of fluid [cal/cm · s · k]
k_H, k_H^k	Hydrogen chain transfer rate constant
k_M, k_M^k	Monomer chain transfer rate constant
k_p, k_p^k	Propagation rate constant [L/mol-sites · s]
k_s	External film mass transfer coefficient [cm/s]
M	Monomer concentration
M_c	Monomer concentration at catalyst surface
M_{eq}	Monomer concentration at surface of microparticle
M_1	Monomer concentration in pores of macroparticle
M_n, M_n^k	Number average molecular weight
M_w, M_w^k	Weight average molecular weight
M_S	Monomer concentration at macroparticle surface
M_i	Concentration of dead polymer of length i
MW	Molecular weight of monomer
ΔM	Concentration drop across external film [mol/L]
p	Pressure
P_i	Concentration of live polymer of length i
Q, Q^k	Polydispersity = M_w/M_n
r	Microparticle radial coordinate
r_1	Macroparticle radial coordinate
r_c	Catalyst microparticle radius
R	Gas constant = 1.987 cal/mol · K
R_c	Radius of catalyst macroparticle
R_1	Radius of macroparticle
R_p	Reaction rate [(g or mol)/g-cat · h]
R_{ob}	Observed polymerization rate [g/g-cat · h]
R_s	Radius of microparticle
R_v	Volumetric reaction rate in macroparticle [mol/L · s]
$t_{1/2}$	Catalyst half-life
T	Temperature
ΔT	Temperature rise across external film
u	Particle-fluid relative velocity
w_k	Weight fraction
x	Chain length
Y_2	Yield after two-hour polymerization

GREEK SYMBOLS

α, α_k	Probability of propagation
ϵ	Porosity
η_s	Microparticle effectiveness factor
η_1	Macroparticle effectiveness factor
θ_k	Fraction of active sites
λ_ℓ, λ_ℓ^k	Moments of live polymer
Λ_ℓ, Λ_ℓ^k	Moments of dead polymer
ν_n, ν_n^k	Number average chain length
ρ	Density
τ_c	Characteristic time for site activation
ϕ_g	Microparticle growth factor = R_s/r_c
Φ_g	Macroparticle growth factor = R_1/R_c

We are grateful to the National Science Foundation and to the industrial sponsors of the University of Wisconsin Polymerization Reaction Engineering Laboratory for research support. We are also indebted to Kyu-Yong Choi for his contributions to our study of these problems.

References

1. E. J. Nagel, V. A. Kirillov, and W. H. Ray, *I.& E.C. Prod. Res. Dev.*, **19**, 372 (1980).
2. T. W. Taylor, K. Y. Choi, H. Yuan, and W. H. Ray, in *Transition Metal Catalyzed Polymerizations*, R. P. Quirk, ed., Harwood Academic Publishers, NY, 1983.
3. K. Y. Choi, T. W. Taylor, and W. H. Ray, *Physical Transport Influences on the Catalyzed Polymerization of Olefins*, Proceedings 1982 IUPAC Meeting, Amherst, MA, p. 240.
4. S. Floyd, K. Y. Choi, T. W. Taylor, and W. H. Ray, *J. Appl. Polym. Sci.*, **32**, 2231 (1986).
5. S. Floyd, K. Y. Choi, T. W. Taylor, and W. H. Ray, *J. Appl. Polym. Sci.*, **32**, 2935 (1986).
6. S. Floyd, G. E. Mann, and W. H. Ray, paper presented at International Symposium on Future Aspects of Olefin Polymerization, July, 1985, Tokyo, Japan.
7. H. G. Yuan, T. W. Taylor, K. Y. Choi, and W. H. Ray, *J. Appl. Polym. Sci.*, **27**, 1691 (1982).
8. C. W. Hock, *J. Polym. Sci. A-1*, **4**, 3055 (1966).
9. R. J. L. Graff, G. Kortleve, and C. G. Vonk, *Polym. Lett.*, **8**, 735 (1970).
10. G. D. Bukatov, V. I. Zaikovskii, V. A. Zakharov, G. N. Kryukova, V. B. Fenelonov, and R. G. Zagrafskaya, *Vysokomol. Soyed. A24*, **3**, 542 (1982).
11. W. H. Ray, *J. Macromol. Sci. Revs. Macromol. Chem.*, **C8 (8)**, 1 (1972).
12. W. H. Ray and R. L. Laurence, in *Chemical Reactor Theory*, Prentice-Hall, Englewood Cliffs, NJ, 1977.
13. T. Keii, Y. Doi, E. Suzuki, M. Tamura, M. Murata, and K. Soga, *Makromol. Chem.*, **185**, 1537 (1984).
14. Heiskanen, T., Doctorate thesis, Helsinki, Finland (1985).
15. R. Galvan and M. Tirrell, paper at 1985 Chicago ACS Meeting.
16. S. Floyd, Ph.D. thesis, University of Wisconsin (1986).
17. B. A. Finlayson, *Nonlinear Analysis in Chemical Engineering*, McGraw-Hill, New York, 1980.
18. J. J. Dongarra, J. R. Bunch, C. B. Moler, and G. W. Stewart, *LINPACK User's Guide*, SIAM, Philadelphia, 1979.
19. K. Y. Choi and W. H. Ray, *J. Appl. Polym. Sci.*, **30**, 1065 (1985).
20. Y. Doi, M. Murata, K. Yano, and T. Keii, *Ind. Eng. Chem. Prod. Res. Dev.*, **21**, 580 (1982).
21. T. Keii, E. Suzuki, M. Tamura, M. Murata, and Y. Doi, *Makromol. Chem.*, **183** (10), 2285 (1982).
22. P. Galli, L. Luciani, and G. Cecchin, *Makromol. Chem.*, **94**, 63 (1981).
23. H. Meyer and K. H. Reichert, *Angew. Makromol. Chem.*, **57**, 211 (1977).
24. D. G. Boucher, I. W. Parsons, and R. N. Haward, *Makromol. Chem.*, **175**, 3461 (1974).
25. P. Pino and B. Rotzinger, *Makromol. Chem. Suppl.*, **7**, 41 (1984).
26. V. A. Zakharov, S. I. Makhtarulin, and Yu. I. Yermakov, *React. Kinet. Catal. Lett.*, **9**, (2), 137 (1978).
27. V. A. Zakharov, V. N. Druzhkov, E. G. Kushnareva, and Yu. I. Yermakov, *Kinetika i Kataliz*, **15** (2), 446 (1974).
28. I. W. Parsons, A. D. Caunt, R. N. Haward, J. A. Licchelli, and M. R. Y. Al-Hillo in *Transition Metal Catalyzed Polymerizations*, R. P. Quirk, ed., Harwood Academic Publishers, New York, 1983.
29. T. Keii, *Kinetics of Ziegler-Natta Polymerization*, Chapman and Hall, London, 1972.
30. A. A. Baulin, A. G. Rodionov, S. S. Ivanchev, and N. M. Domareva, *Europ. Polym. J.*, **16**, 937 (1980).
31. A. A. Baulin, A. G. Rodionov, S. S. Ivanchev, T. V. Kreitser, and A. L. Gol'denberg, *Vysokomol. Soyed.*, **A22 (7)**, 1486 (1980).
32. L. L. Bohm, *Makromol. Chem.*, **89**, 1 (1980).
33. Z. W. Wilchinsky, R. W. Looney, and E. G. M. Tornqvist, *J. Catal.*, **28**, 351 (1973).
34. H. Schnecko, W. Dost, and W. Kern, *Makromol. Chem.*, **121**, 159 (1969).
35. K. H. Reichert, H. Franz and N. Guentherburg, paper presented at IUPAC 28th Macromolecular Symposium, Amherst, MA (1982).
36. C. W. Hock, *J. Polym. Sci. A-1*, **4**, 3055 (1966).
37. J. Wristers, *J. Polym. Sci. Polym. Phys. Ed.*, **11**, 1619 (1973).

38. U.S. Patent 3,887,454 (1975), to Phillips.
39. French Patent 2,067,413 (1971), to National Distillers.
40. U.S. Patent 3,709,853 (1973), to Union Carbide.
41. U.S. Patent 3,050,514 (1962), to Allied Chemical.
42. U.S. Patent 3,960,826 (1976), to National Petrochemicals.
43. U.S. Patent 4,349,648 (1982), to Union Carbide.
44. K. Soga, K. Izumi, M. Terano, and S. Ikeda, *Makromol. Chem.*, **181**, 657 (1980).
45. U.S. Patent 4,210,738 (1980), to Solvay.
46. R. P. Nielsen, in *Transition Metal Catalyzed Polymerizations*, R. P. Quirk, Ed., Harwood Academic, New York, 1983.
47. A. A. Baulin, A. S. Semenova, L. G. Stefanovich, N. M. Chirkov, and A. V. Stafeyev, *Vysokomol. Soyed.*, **A16**, 2688 (1974).
48. V. R. Gurevitch, M. A. Dalin, and L. Ya. Vedeneeva, *Azerb. Khim. Zh.*, **6**, 37 (1963).
49. A. A. Baulin, V. N. Sokolov, A. S. Semenova, N. M. Chirkov, and L. F. Shalayeva, *Vysokomol. Soyed.*, **A17 (1)**, 46 (1975).
50. S. S. Ivanchev, A. A. Baulin, and A. G. Rodionov, *J. Polym. Sci. Polym. Schem. Ed.*, **18**, 2045 (1980).
51. G. E. Mann, M. S. thesis, University of Wisconsin (1985).
52. N. F. Brockmeier and J. B. Rogan, paper presented at A.I.Ch.E. Meeting, Anaheim, CA (May, 1984).
53. A. Munoz-Escalona and A. Parada, *Polymer*, **20**, 474 (1979).
54. B. M. Grieveson, *Makromol. Chem.*, **84**, 93 (1965).
55. V. A. Zakhavrov, Z. K. Bukatova, S. I. Makhtarulin, N. B. Chumaevskii, and Yu. I. Yermakov, *Vysokomol. Soyed.*, **A21 (3)**, 496 (1979).
56. V. A. Zakharov, N. B. Chumaevskii, Z. K. Bulatova, G. D. Bukatov, and Yu. I. Yermakov, *React. Kinet. Catal. Lett.*, **5** (4), 429 (1976).
57. E. Suzuki, M. Tamura, Y. Doi, and T. Keii, *Makromol. Chem.*, **180**, 2235 (1979).
58. N. Kashiwa and J. Yoshitake, *Makromol. Chem. Rapid Commun.*, **3**, 211 (1982).
59. L. L. Bohm and H. Passing, *Makromol. Chem.*, **177**, 1097 (1976).
60. J. C. W. Chien, *J. Polym. Sci. Polym. Chem. Ed.*, **17**, 2555 (1979).
61. D. Singh and R. P. Merrill, *Macromolecules*, **4** (5), 599 (1971).
62. V. W. Buls and T. L. Higgins, *J. Polym. Sci. A-1*, **8**, 1037 (1970).
63. J. R. Crabtee, F. N. Grimsby, A. J. Nummelin, and J. M. Sketchley, *J. Appl. Polym. Sci.*, **17**, 959 (1973).
64. U. Zucchini and G. Cecchin, *Adv. Polym. Sci.*, **51**, 101 (1983).
65. M. N. Berger, G. Boocock, and R. N. Haward, *Adv. Catal.*, **19**, 211 (1969).
66. L. A. M. Rodriguez and H. M. Van Looy, *J. Polym. Sci. A-1*, **4**, 1971 (1966).
67. T. Keii, E. Suzuki, M. Tamura, and Y. Doi, in *Transition Metal Catalyzed Polymerizations*, R. P. Quirk, Ed., Harwood Academic, New York, 1983.
68. L. A. Rishina and E. I. Vizen, *Europ. Polym. J.*, **16**, 965 (1980).
69. J. C. W. Chien, *J. Polym. Sci. A*, **1**, 1839 (1963).
70. L. L. Bohm, *Polymer*, **19**, 562 (1979).
71. T. J. Pullukat, M. Shida, and R. E. Hoff, Proceedings of the 1981 MMI Symposium on Transition Metal Catalyzed Polymerizations, Midland, MI.
72. R. E. Hoff and M. Shida, *J. Appl. Polym. Sci.*, **17**, 3003 (1973).
73. Ye. I. Vizen and F. I. Yakobson, *Vysokomol. Soyed.*, *A20*, **(4)** 927 (1978).
74. A. A. Buniyat-Zade, T. M. Kasimov, A. B. Nasirova, R. T. Gandilov, and Ya. M. Bilalov, *Azerb. Khim. Zh.*, **1**, 98 (1980).
75. W. C. Taylor and L. H. Tung, *Polym Lett.*, **1**, 157 (1963).
76. A. A. Baulin, L. F. Shalayeva, and S. S. Ivanchev, *Dokl. Akad. Nauk SSSR*, **231**, 413 (1976).
77. T. Heiskanen and W. H. Ray, *The Copolymerization of Olefins Over Ziegler Natta Catalysts* (paper in preparation).
78. Japan Patent 79 160,489 (1979), to Chisso Corp.
79. U.S. Patent 3,678,025 (1972), to Dow Chemical.
80. U.S. Patent 3,899,477 (1975), to Monsanto.
81. U.S. Patent 4,031,298 (1977), to Chemplex.
82. U.S. Patent 4,109,071 (1978), to Solvay.

83. U.S. Patent 4,154,701 (1979), to Amoco.
84. U.S. Patent 4,210,559 (1982), to Amoco.
85. Japan Patent 72 42980 (1972), to Asahi Chemical Industries.
86. U.S. Patent 4,349,648 (1982), to Union Carbide.
87. U.S. Patent 4,354,009 (1982), to Union Carbide.
88. U.S. Patent 3,859,267 (1975), to Mitsubishi Chemical Industries.

Received June 7, 1986
Accepted June 13, 1986